Eur. Phys. J. C (2019) 79:368
https://doi.org/10.1140/epjc/s10052-019-6863-8

THE EUROPEAN PHYSICAL JOURNAL C

Regular Article - Experimental Physics

Measurement of the $\mathrm{t\bar{t}}$ production cross section, the top quark mass, and the strong coupling constant using dilepton events in pp collisions at $\sqrt{s} = 13\,\text{TeV}$

CMS Collaboration*

CERN, 1211 Geneva 23, Switzerland

Received: 26 December 2018 / Accepted: 6 April 2019 / Published online: 29 April 2019

Abstract A measurement of the top quark–antiquark pair production cross section $\sigma_{\mathrm{t\bar{t}}}$ in proton–proton collisions at a centre-of-mass energy of 13 TeV is presented. The data correspond to an integrated luminosity of $35.9\,\text{fb}^{-1}$, recorded by the CMS experiment at the CERN LHC in 2016. Dilepton events ($\mathrm{e}^{\pm}\mu^{\mp}$, $\mu^{+}\mu^{-}$, $\mathrm{e}^{+}\mathrm{e}^{-}$) are selected and the cross section is measured from a likelihood fit. For a top quark mass parameter in the simulation of $m_{\mathrm{t}}^{\mathrm{MC}} = 172.5\,\text{GeV}$ the fit yields a measured cross section $\sigma_{\mathrm{t\bar{t}}} = 803 \pm 2\,(\text{stat}) \pm 25\,(\text{syst}) \pm 20\,(\text{lumi})\,\text{pb}$, in agreement with the expectation from the standard model calculation at next-to-next-to-leading order. A simultaneous fit of the cross section and the top quark mass parameter in the POWHEG simulation is performed. The measured value of $m_{\mathrm{t}}^{\mathrm{MC}} = 172.33 \pm 0.14\,(\text{stat})\,^{+0.66}_{-0.72}\,(\text{syst})\,\text{GeV}$ is in good agreement with previous measurements. The resulting cross section is used, together with the theoretical prediction, to determine the top quark mass and to extract a value of the strong coupling constant with different sets of parton distribution functions.

1 Introduction

Measurements of the top quark–antiquark pair cross section $\sigma_{\mathrm{t\bar{t}}}$ in proton–proton (pp) collisions provide important tests of the standard model (SM). At the CERN LHC, measurements with increasing precision have been performed by the ATLAS and CMS Collaborations in several different decay channels and at four pp collision energies [1–5]. Precise theoretical predictions of $\sigma_{\mathrm{t\bar{t}}}$ have been performed in perturbative quantum chromodynamics (QCD) at next-to-next-to-leading order (NNLO) [6–9]. The calculations depend on several fundamental parameters: the top quark mass m_{t}, the strong coupling constant α_S, and the parton distribution functions (PDFs) of the proton. The measurements of $\sigma_{\mathrm{t\bar{t}}}$ have been used to determine the top quark pole mass [1,4,10–12], α_S [4,13], and the PDFs [14–17].

The value of m_{t} significantly affects the prediction for many observables, either directly or via radiative corrections. It is a key input to electroweak precision fits [18] and, together with the value of the Higgs boson mass and α_S, it has direct implications on the SM predictions for the stability of the electroweak vacuum [19]. In QCD calculations beyond leading order, m_{t} depends on the renormalization scheme. In the context of the $\sigma_{\mathrm{t\bar{t}}}$ predictions, the pole (on-shell) definition for the top quark mass $m_{\mathrm{t}}^{\mathrm{pole}}$ has wide applications; however, it suffers from the renormalon problem that introduces a theoretical ambiguity in its definition. The minimal subtraction ($\overline{\mathrm{MS}}$) renormalization scheme has been shown to have a faster convergence than other schemes [20]. The relation between the pole and $\overline{\mathrm{MS}}$ masses is known to the four-loop level in QCD [21]. Experimentally, the most precise measurements of the top quark mass are obtained in so-called direct measurements performed at the Tevatron and LHC [22–25]. Except for a few cases such as Ref. [26], the measurements rely on Monte Carlo (MC) generators to provide the relation between the top quark mass and an experimental observable. Current MC generators implement matrix elements at leading or next-to-leading order (NLO), while higher orders are simulated through parton showering. Studies suggest that the top quark mass parameter $m_{\mathrm{t}}^{\mathrm{MC}}$, as implemented in current MC generators, corresponds to $m_{\mathrm{t}}^{\mathrm{pole}}$ to an uncertainty on the order of 1 GeV [27,28]. A theoretically well-defined mass can be determined by comparing the measured $\mathrm{t\bar{t}}$ cross section to the fixed-order theoretical predictions [1,4,10–12].

With the exception of the quark masses, α_S is the only free parameter in the QCD Lagrangian. While the renormalization group equation predicts the energy dependence of α_S, i.e. it gives a functional form for $\alpha_S(Q)$, where Q is the energy scale of the process, actual values of α_S can only be obtained from experimental data. By convention and to facilitate comparisons, α_S values measured at different

G. Vesztergombi, A. C. Benvenuti: Deceased.

* e-mail: cms-publication-committee-chair@cern.ch

energy scales are typically evolved to $Q = m_Z$, the mass of the Z boson. The current world-average value for $\alpha_S(m_Z)$ is 0.1181 ± 0.0011 [29]. In spite of this relatively precise result, the uncertainty in α_S still contributes significantly to many QCD predictions, including cross sections for top quark or Higgs boson production. Very few measurements allow α_S to be tested at high Q, and the precision on the world-average value for $\alpha_S(Q)$ is driven by low-Q measurements. A determination of $\sigma_{\mathrm{t\bar{t}}}$ was used by the CMS Collaboration to extract the value of $\alpha_S(m_Z)$ at NNLO for the first time [11]. In the prediction for $\sigma_{\mathrm{t\bar{t}}}$, α_S appears not only in the expression for the parton-parton interaction but also in the QCD evolution of the PDFs. Varying the value of $\alpha_S(m_Z)$ in the $\sigma_{\mathrm{t\bar{t}}}$ calculation therefore requires a consistent modification of the PDFs. The full correlation between the gluon PDF, α_S, and m_{t} in the prediction for $\sigma_{\mathrm{t\bar{t}}}$ has to be accounted for.

The analysis uses events in the dileptonic decay channels in which the two W bosons from the electroweak decays of the two top quarks each produce an electron or a muon, leading to three event categories: $\mathrm{e}^{\pm}\mu^{\mp}$, $\mu^{+}\mu^{-}$, and $\mathrm{e}^{+}\mathrm{e}^{-}$. The data set was recorded by CMS in 2016 at a centre-of-mass energy of 13 TeV, corresponding to an integrated luminosity of $35.9\,\mathrm{fb}^{-1}$. The measurement is performed using a maximum-likelihood fit in which the sources of systematic uncertainty are treated as nuisance parameters. Distributions of observables are chosen as input to the fit so as to further constrain the uncertainties. The fitting procedure largely follows the approach of Ref. [4]. In this analysis, the number of events is significantly larger than in previous data sets, thus providing tighter constraints. The dominant uncertainties come from the integrated luminosity and the efficiency to identify the two leptons. The correlation between the three decay channels is used to constrain the overall lepton identification uncertainty to that of the better-constrained lepton, which is the muon.

Experimentally, the measured value of $\sigma_{\mathrm{t\bar{t}}}$ has a residual dependence on the value of $m_{\mathrm{t}}^{\mathrm{MC}}$ used in the simulation to estimate the detector efficiency and acceptance. In contrast, the experimental dependence of $\sigma_{\mathrm{t\bar{t}}}$ on the value of $\alpha_S(m_Z)$ used in the simulation is negligible [11]. For the extraction of a theoretically well-defined m_{t}, the dependence of the cross section on the assumption of a $m_{\mathrm{t}}^{\mathrm{MC}}$ value can be reduced by including $m_{\mathrm{t}}^{\mathrm{MC}}$ as an additional free parameter in the fit [30]. In this paper, the cross section $\sigma_{\mathrm{t\bar{t}}}$ is first measured for a fixed value of $m_{\mathrm{t}}^{\mathrm{MC}} = 172.5$ GeV, and then determined simultaneously with $m_{\mathrm{t}}^{\mathrm{MC}}$. In the simultaneous fit, input distributions sensitive to the top quark mass are introduced in order to constrain $m_{\mathrm{t}}^{\mathrm{MC}}$. For the measured parameter $m_{\mathrm{t}}^{\mathrm{MC}}$, the same systematic uncertainties are taken into account as in Ref. [31]. Finally, the measured value of $\sigma_{\mathrm{t\bar{t}}}$ at the experimentally constrained value of $m_{\mathrm{t}}^{\mathrm{MC}}$ is used to extract $\alpha_S(m_Z)$ and m_{t} in the $\overline{\mathrm{MS}}$ scheme, using different PDF sets. For m_{t}, the pole mass scheme is also considered.

The paper is structured as follows. After a brief description of the CMS experiment and the MC event generators in Sect. 2, the event selection is presented in Sect. 3. The event categories and the maximum-likelihood fit are explained in Sect. 4. The systematic uncertainties in the measurement are discussed in Sect. 5. The result of the cross section measurement at a fixed value of $m_{\mathrm{t}}^{\mathrm{MC}} = 172.5$ GeV is presented in Sect. 6, and the simultaneous measurement of $\sigma_{\mathrm{t\bar{t}}}$ and $m_{\mathrm{t}}^{\mathrm{MC}}$ is presented in Sect. 7. The extraction of m_{t} and α_S in the $\overline{\mathrm{MS}}$ scheme and the top quark pole mass are described in Sects. 8 and 9, respectively, and a summary is given in Sect. 10.

2 The CMS detector and Monte Carlo simulation

The central feature of the CMS apparatus [32] is a superconducting solenoid of 6 m internal diameter, providing a magnetic field of 3.8 T. Within the solenoid volume are a silicon pixel and strip tracker, a lead tungstate crystal electromagnetic calorimeter, and a brass and scintillator hadron calorimeter, each composed of a barrel and two endcap sections. These are used to identify electrons, photons, and jets. Forward calorimeters extend the pseudorapidity coverage provided by the barrel and endcap detectors. Muons are detected in gas-ionization chambers embedded in the steel flux-return yoke outside the solenoid. The detector is nearly hermetic, providing reliable measurement of the momentum imbalance in the plane transverse to the beams. A two-level trigger system selects interesting events for offline analysis [33]. A more detailed description of the CMS detector, together with a definition of the coordinate system used and the relevant kinematic variables, can be found in Ref. [32].

The POWHEG v2 [34–36] NLO MC generator is used to simulate $\mathrm{t\bar{t}}$ events [37] and its model dependencies on $m_{\mathrm{t}}^{\mathrm{MC}}$, the PDFs [37], and the renormalization and factorization scales, $\mu_{\mathrm{r}} = \mu_{\mathrm{f}} = m_{\mathrm{T}} = \sqrt{m_{\mathrm{t}}^2 + p_{\mathrm{T}}^2}$, where m_{t} is the pole mass and p_{T} is the transverse momentum of the top quark. The PDF set NNPDF3.0 [38] is used to describe the proton structure. The parton showers are modelled using PYTHIA 8.2 [39] with the CUETP8M2T4 underlying event (UE) tune [40,41]. In this analysis, $\mathrm{t\bar{t}}$ events are split into a signal and a background component. The signal consists of dilepton events and includes contributions from leptonically decaying τ leptons. All other $\mathrm{t\bar{t}}$ events are considered as background.

Contributions to the background include single top quark processes (tW), Drell–Yan (DY) events (Z/γ^*+jets), and W+jets production, as well as diboson (VV) events (including WW, WZ, and ZZ) with multiple jets, while the contribution from QCD multijet production is found to be negligible. The DY and tW processes are simulated in POWHEG v2 [42–44] with the NNPDF3.0 PDF and interfaced to PYTHIA 8.202 with the UE tune CUETP8M2T4 [45] for

hadronization and fragmentation. The W+jets events are generated at NLO using MADGRAPH5_aMC@NLO 2.2.2 [46,47] with the NNPDF3.0 PDF and PYTHIA 8.2 with the UE tune CUETP8M1. Events with WW, WZ, and ZZ diboson processes are generated at leading order using PYTHIA 8.2 with the NNPDF2.3 PDF and the CUETP8M1 tune.

To model the effect of additional pp interactions within the same or nearby bunch crossing (pileup), simulated minimum bias interactions are added to the simulated data. Events in the simulation are then weighted to reproduce the pileup distribution in the data, which is estimated from the measured bunch-to-bunch instantaneous luminosity, assuming a total inelastic pp cross section of 69.2 mb [48].

For comparison with the measured distributions, the event yields in the simulated samples are normalized to their cross section predictions. These are obtained from calculations at NNLO (for W+jets and Z/γ^*+jets [49]), NLO plus next-to-next-to-leading logarithms (NNLL) (for tW production [50]), and NLO (for diboson processes [51]). For the simulated $\mathrm{t\bar{t}}$ sample, the full NNLO+NNLL calculation, performed with the TOP++ 2.0 program, is used [52]. The proton structure is described by the CT14nnlo [53] PDF set, where the PDF and α_S uncertainties are estimated using the prescription by the authors. These are added in quadrature to the uncertainties originating from the scale variation $m_\mathrm{t}/2 < \mu_\mathrm{r}, \mu_\mathrm{f} < 2m_\mathrm{t}$. The cross section prediction is $\sigma_{\mathrm{t\bar{t}}}^{\mathrm{theo}} = 832\,^{+20}_{-29}\,(\mathrm{scale}) \pm 35\,(\mathrm{PDF}+\alpha_S)$ pb, assuming a top quark pole mass of 172.5 GeV.

3 Event selection

Events with at least two leptons (electron or muon) of opposite charge are selected. In events with more than two leptons, the two leptons of opposite charge with the highest p_T are used. An event sample of three mutually exclusive event categories $\mathrm{e}^\pm\mu^\mp$, $\mu^+\mu^-$, and $\mathrm{e}^+\mathrm{e}^-$ is obtained.

A combination of single and dilepton triggers is used to collect the events. Each event is required to pass at least one of the triggers described below. Events in the $\mathrm{e}^\pm\mu^\mp$ channel are required to contain either one electron with $p_\mathrm{T} > 12$ GeV and one muon with $p_\mathrm{T} > 23$ GeV, or one electron with $p_\mathrm{T} > 23$ GeV and one muon with $p_\mathrm{T} > 8$ GeV. Events in the same-flavour channels are required to have $p_\mathrm{T} > 23\,(17)$ GeV for the electron (muon) with the higher p_T, referred to in the following as the leading lepton, and $p_\mathrm{T} > 12\,(8)$ GeV for the other electron (muon), referred to as the subleading lepton. For all channels, single-lepton triggers with one electron (muon) with $p_\mathrm{T} > 27\,(24)$ GeV are also used.

The particle-flow (PF) algorithm aims to reconstruct and identify each individual particle in an event, and to form PF candidates by combining information from the various components of the CMS detector [54]. The reconstructed vertex with the largest value of summed physics-object p_T^2 is taken to be the primary pp interaction vertex.

Electron and muon candidates are identified through their specific signatures in the detector [55,56]. Lepton candidates are required to have $p_\mathrm{T} > 25\,(20)$ GeV for the leading (subleading) lepton, in the range $|\eta| < 2.4$. Electron candidates in the transition region between the barrel and endcap calorimeters, corresponding to $1.4442 < |\eta| < 1.5660$, are rejected because the reconstruction of electrons in this region is not optimal.

Lepton isolation requirements are based on the ratio of the scalar sum of the p_T of neighbouring PF candidates to the p_T of the lepton candidate, which is referred to as the lepton isolation variable. These PF candidates are the ones falling within a cone of size $\Delta R = 0.3\,(0.4)$ for electrons (muons), centred on the lepton direction, excluding the contribution from the lepton candidate itself. The cone size ΔR is defined as the square root of the quadrature sum of the differences in the azimuthal angle and pseudorapidity. The value of the isolation variable is required to be smaller than 6% for electrons and 15% for muons. Events with dilepton invariant mass $m_{\ell\ell} < 20$ GeV ($\ell = \mathrm{e}, \mu$) are rejected to suppress backgrounds due to QCD multijet production and decays of low mass resonances. Additionally, leptons are required to be consistent with originating from the primary interaction vertex.

Jets are reconstructed from the PF candidates using the anti-k_T clustering algorithm with a distance parameter of 0.4 [57,58]. The jet momentum is determined from the vectorial sum of all particle momenta in the jet, and is found from simulation to be within 5 to 10% of the true momentum over the relevant phase space of this analysis [59]. Pileup interactions can contribute additional tracks and calorimetric energy depositions to the jet momentum. To mitigate this effect, charged particles identified as originating from pileup vertices are discarded and an offset correction is applied to correct for remaining contributions [59]. The jet energy corrections are determined from measurements of the energy balance in dijet, multijet, photon+jet, and leptonically decaying Z+jets events, and are applied as a function of the jet p_T and η to both data and simulated events [59]. For this measurement, jets are selected if they fulfill the criteria $p_\mathrm{T} > 30$ GeV and $|\eta| < 2.4$.

Jets originating from the hadronization of b quarks (b jets) are identified (b tagged) using the combined secondary vertex [60] algorithm, which combines lifetime information from tracks and secondary vertices. To achieve high purity, a working point is chosen such that the fraction of light-flavour jets with $p_\mathrm{T} > 30$ GeV that are falsely identified as b jets is 0.1%, resulting in an average efficiency of about 41% for genuine b jets and 2.2% for c jets [60].

In the same-flavour channels, $\mu^+\mu^-$ and e^+e^-, DY events are suppressed by excluding the region of the Z boson mass through the requirement $76 < m_{\ell\ell} < 106\,\text{GeV}$. In these channels, events are also required to contain at least one b-tagged jet.

Distributions of the leading and subleading lepton p_T and η, and the jet and b-tagged jet multiplicities in events fulfilling the above selection criteria are shown in Figs. 1, 2 and 3 for the $e^\pm\mu^\mp$, $\mu^+\mu^-$, and e^+e^- channels, respectively. The event yields in the simulations are normalized to the corresponding cross section predictions, as explained in Sect. 2. Selected events include a very small contribution from $t\bar{t}$ processes in the lepton+jets decay channel (referred to as "$t\bar{t}$ other" in the figures) in which one of the charged leptons originates from heavy-flavour hadron decay, misidentified hadrons, muons from light-meson decays, or electrons from unidentified photon conversions. Such leptons also lead to dilepton background in this analysis via W+jets processes.

In all categories, the simulation is found to describe the data well within the systematic uncertainties, indicated by the bands in the figures.

4 Event categories and fit procedure

The measurement is performed using a template fit to multidifferential distributions, divided into distinct event categories using the b-tagged jet multiplicity, similar to the method utilized in a previous measurement [4]. In each of the same-flavour channels, two categories are defined, corresponding to events having 1 or 2 b-tagged jets. Events with zero b-tagged jets are not included since they are dominated by the DY background process. In the $e^\pm\mu^\mp$ channel, three categories are defined, corresponding to events having 1, 2, or 0 or ≥ 3 b-tagged jets. The templates describing the distributions for the signal and background events are taken from simulation. Categorizing the events by their b-tagged jet multiplicity allows the efficiency ϵ_b for selecting and identifying a b jet to be constrained. Previous measurements that used a template fit with dilepton events were restricted to the $e^\pm\mu^\mp$ channel [1,4]. In this analysis, the decay channels with two electrons and two muons are also included in the fit. In this way, additional constraints on the lepton identification efficiencies are obtained.

First, a visible $t\bar{t}$ cross section $\sigma_{t\bar{t}}^{\text{vis}}$, defined for a phase space corresponding to the experimentally accessible fiducial volume, as described in Sect. 6, is determined. For the visible cross section, the fit is used to constrain the systematic uncertainties from the data. Using the relation

$$\sigma_{t\bar{t}} = \frac{\sigma_{t\bar{t}}^{\text{vis}}}{A_{\ell\ell}}, \tag{1}$$

the measured visible cross section is then extrapolated to the full phase space to obtain $\sigma_{t\bar{t}}$. Here, $A_{\ell\ell}$ denotes the acceptance, which is defined as the fraction of $t\bar{t}$ events that fulfill the selection criteria for the visible cross section. The acceptance incorporates the combined branching fraction for the t and $\bar{t}$ quarks to decay to two charged leptons [29]. Apart from the free parameter of interest $\sigma_{t\bar{t}}^{\text{vis}}$, the parameters of the fit are the J nuisance parameters $\boldsymbol{\lambda} = (\lambda_1, \lambda_2, \ldots, \lambda_J)$ corresponding to the various sources of systematic uncertainty, discussed in detail in Sect. 5.

The likelihood function L is based on Poisson statistics:

$$L = \prod_i \frac{e^{-\nu_i}\nu_i^{n_i}}{n_i!} \prod_j \pi(\lambda_j), \tag{2}$$

where i denotes the bin of the respective final-state distribution, and ν_i and n_i are the expected and observed number of events in bin i, respectively. The symbol $\pi(\lambda_j)$ denotes a penalty term for the deviation of the nuisance parameter λ_j from its nominal value according to its prior density distribution. A Gaussian prior density distribution is assumed for all nuisance parameters. The expectation values ν_i can be written as

$$\nu_i = s_i(\sigma_{t\bar{t}}^{\text{vis}}, \boldsymbol{\lambda}) + \sum_k b_{k,i}^{\text{MC}}(\boldsymbol{\lambda}). \tag{3}$$

Here, s_i denotes the expected number of $t\bar{t}$ signal events in bin i and the quantity $b_{k,i}^{\text{MC}}$ represents the prediction of the number of background events in bin i from source k. The MINUIT program [61] is used to minimize $-2\ln(L)$ with L given in Eq. (2), and the MINOS [61] algorithm is used to estimate the uncertainties.

For the determination of the b tagging efficiencies, multinomial probabilities are used to describe the expected number of signal events with one b-tagged jet, s_{1b}, two b-tagged jets, s_{2b}, and zero or more than two b-tagged jets, s_{other}:

$$s_{1b} = \mathcal{L}\sigma_{t\bar{t}}^{\text{vis}}\epsilon_{\ell\ell}2\epsilon_b(1 - C_b\epsilon_b), \tag{4}$$

$$s_{2b} = \mathcal{L}\sigma_{t\bar{t}}^{\text{vis}}\epsilon_{\ell\ell}\epsilon_b^2 C_b, \tag{5}$$

$$s_{\text{other}} = \mathcal{L}\sigma_{t\bar{t}}^{\text{vis}}\epsilon_{\ell\ell}(1 - 2\epsilon_b(1 - C_b\epsilon_b) - \epsilon_b^2 C_b), \tag{6}$$

where $\mathcal{L}$ denotes the integrated luminosity and $\epsilon_{\ell\ell}$ is the efficiency for events in the visible phase space to pass the full selection described in Sect. 3. The quantity C_b corrects for any small correlations between the tagging of two b jets in an event, expressed as $C_b = 4s_{\text{all}}s_{2b}/(s_{1b} + 2s_{2b})^2$, where s_{all} denotes the total number of signal events. The values for $\epsilon_{\ell\ell}$, ϵ_b, and C_b are directly determined from the $t\bar{t}$ signal simulation, expressing ϵ_b as $(s_{1b} + 2s_{2b})/2s_{\text{all}}$. The values of these parameters for the nominal signal simulation in the $e^\pm\mu^\mp$ channel are $\epsilon_{e\mu} = 0.49$, $\epsilon_b = 0.30$, and $C_b = 1.00$.

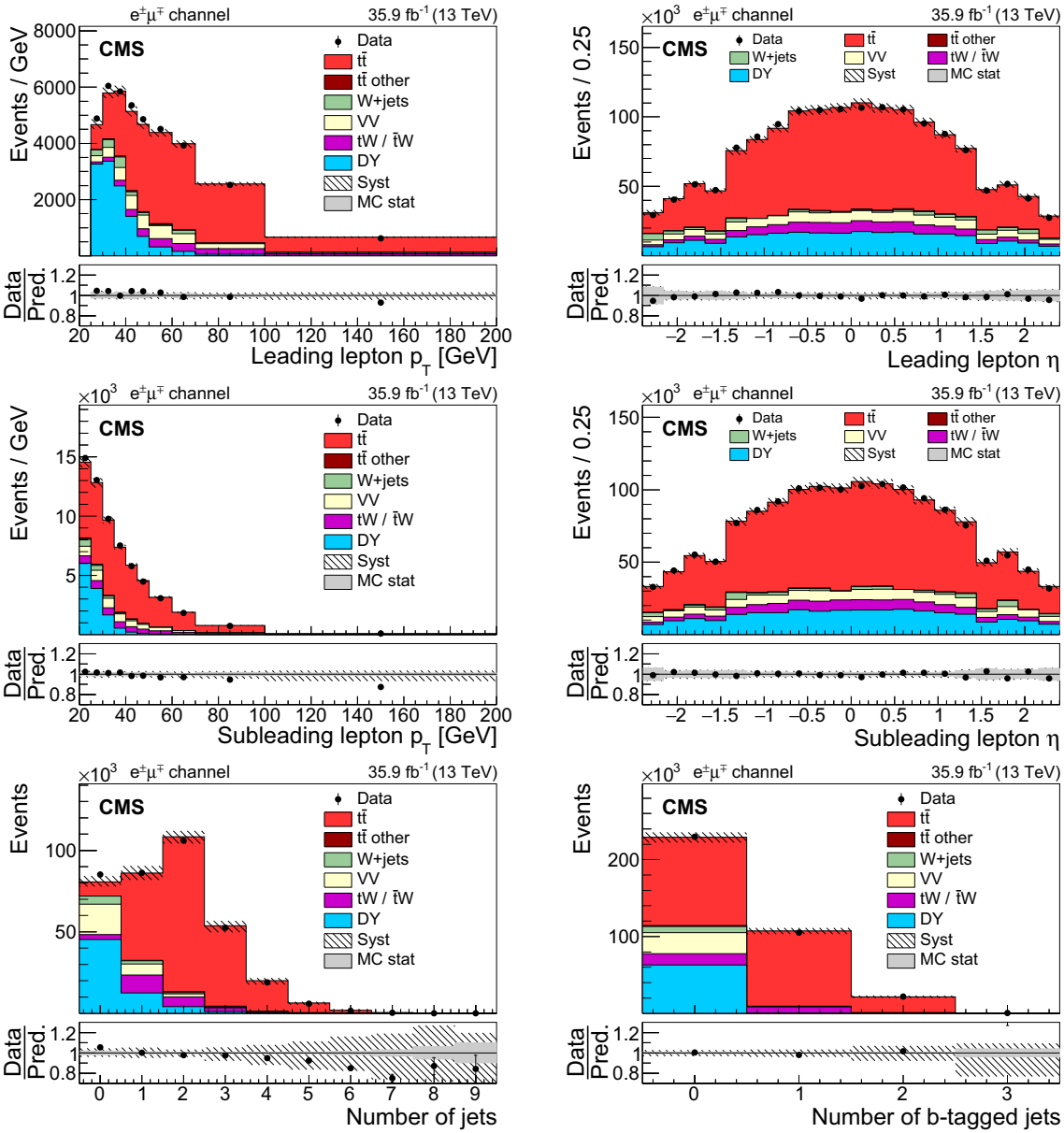

Fig. 1 Distributions of the transverse momentum (left) and pseudo-rapidity (right) of the leading (upper) and subleading (middle) leptons in the $e^{\pm}\mu^{\mp}$ channel after the event selection for the data (points) and the predictions for the signal and various backgrounds from the simulation (shaded histograms). The lower row shows the jet (left) and b-tagged jet (right) multiplicity distributions. The vertical bars on the points represent the statistical uncertainties in the data. The hatched bands correspond to the systematic uncertainty in the $t\bar{t}$ signal MC simulation. The uncertainties in the integrated luminosity and background contributions are not included. The ratios of the data to the sum of the predicted yields are shown in the lower panel of each figure. Here, the solid gray band represents the contribution of the statistical uncertainty in the MC simulation

The overall selection efficiency $\epsilon_{\ell\ell}$ is a linear combination of the efficiencies $\epsilon_{e\mu}$, ϵ_{ee}, and $\epsilon_{\mu\mu}$, in the three different dilepton channels, each given by the product of the two efficiencies for identifying a single lepton of the respective flavour. Prior to the fit, the muon identification uncertainty is smaller than that for electrons. By fitting the three dilepton decay channels simultaneously, the ratio of single-lepton efficiencies ϵ_e and ϵ_μ is constrained. In the fit, the electron identification uncertainty is constrained to that for muons.

The values for $\epsilon_{\ell\ell}$, ϵ_b, C_b, the number of signal events in each category, and the background rates depend on the nuisance parameters $\boldsymbol{\lambda}$. The dependence on the parameter λ_j is modelled by a second-order polynomial that describes the quantity at the three values $\lambda_j = 0, 1, -1$, corresponding to

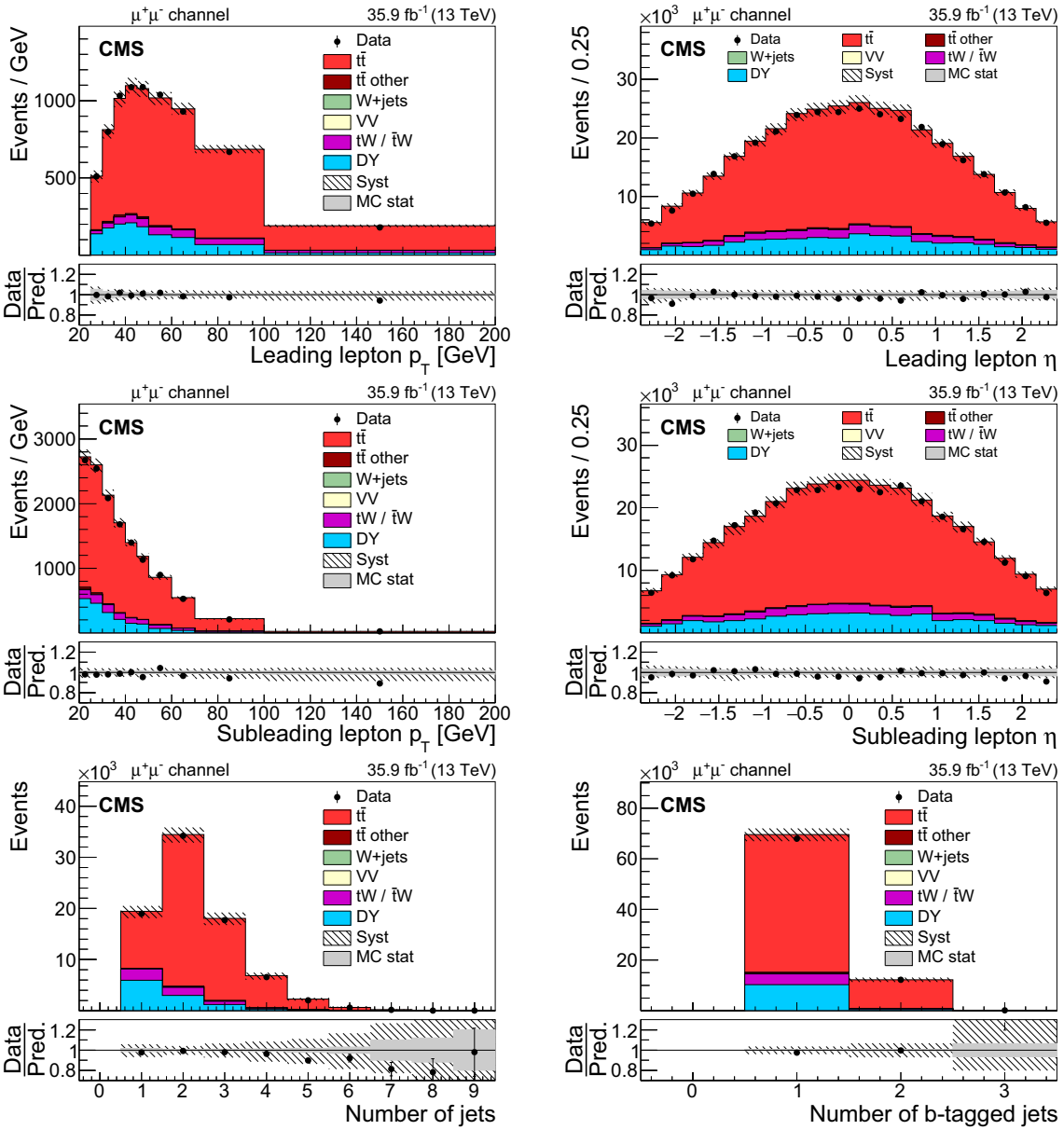

Fig. 2 The same distributions as in Fig. 1, but for the $\mu^+\mu^-$ channel

the nominal value of the parameter and to a variation by +1 and − 1 standard deviation, respectively. If a variation is only possible in one direction, a linear function is used to model the dependence on λ_j.

The events are further categorized by the number of additional non-b-tagged jets in the event. Each of the seven previously described event categories is further divided by grouping together events with 0, 1, 2, or ≥ 3 additional non-b-tagged jets, thus producing 28 disjoint event categories. For those categories that have events with at least one additional non-b-tagged jet, the smallest p_{T} among those jets is used as the observable in the fit. For those categories containing events with zero additional non-b-tagged jets, the total number of events in the category is used as the observable in the fit. The further division of events into these categories and the observable distributions from each category provide the sensitivity to constrain the modelling systematic uncertainties, such as those coming from variations in the scales for the matrix element (ME) and parton shower (PS) matching. For events with no additional jets, the total event yield is used.

The statistical uncertainty in the templates from simulation is taken into account by using pseudo-experiments. At each iteration, templates are varied within their statistical uncertainty. Templates created from different simulations are treated as statistically uncorrelated, while templates derived by varying weights in the simulation are treated as correlated.

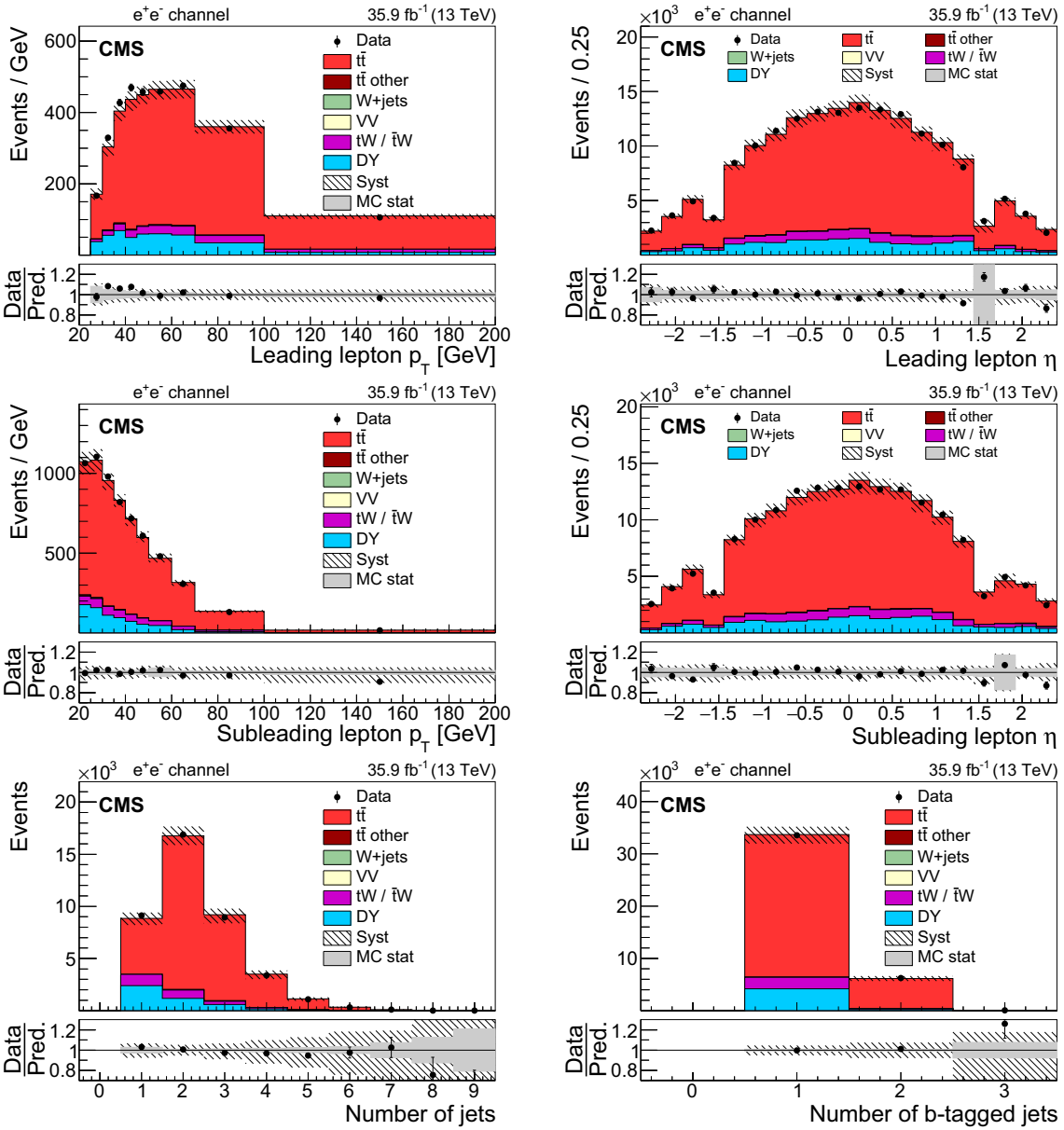

Fig. 3 The same distributions as in Fig. 1, but for the e^+e^- channel

The template dependencies are rederived and the fit to data is repeated. Repeating this 30,000 times yields an approximately Gaussian distribution of the fitted value of the $t\bar{t}$ cross section (and of m_t^{MC} in the combined fit) and of the vast majority of the nuisance parameters. The root-mean-square of each distribution is considered as an additional uncertainty from the event counts in the simulated samples for the corresponding nuisance parameter.

The input distributions to the fit are shown in Figs. 4, 5 and 6, where the data are compared to the signal and background distributions resulting from the fit to the data. In the top row, the number of events without additional non-b-tagged jets is displayed. For events with at least one additional non-b-tagged jet, the p_T distributions of the non-b-tagged jet with the smallest p_T in the respective category is considered, except for the category corresponding to events with 2 b-tagged jets and at least three additional non-b-tagged jets, where the statistical uncertainty of the simulation is high. This distribution is chosen in order to constrain the jet energy scale at lower jet p_T, where the corresponding systematic uncertainty is larger [59]. Good agreement is found between the data and the simulation.

5 Systematic uncertainties

The contributions from each source of systematic uncertainty are represented by nuisance parameters (see Sect. 4). For each

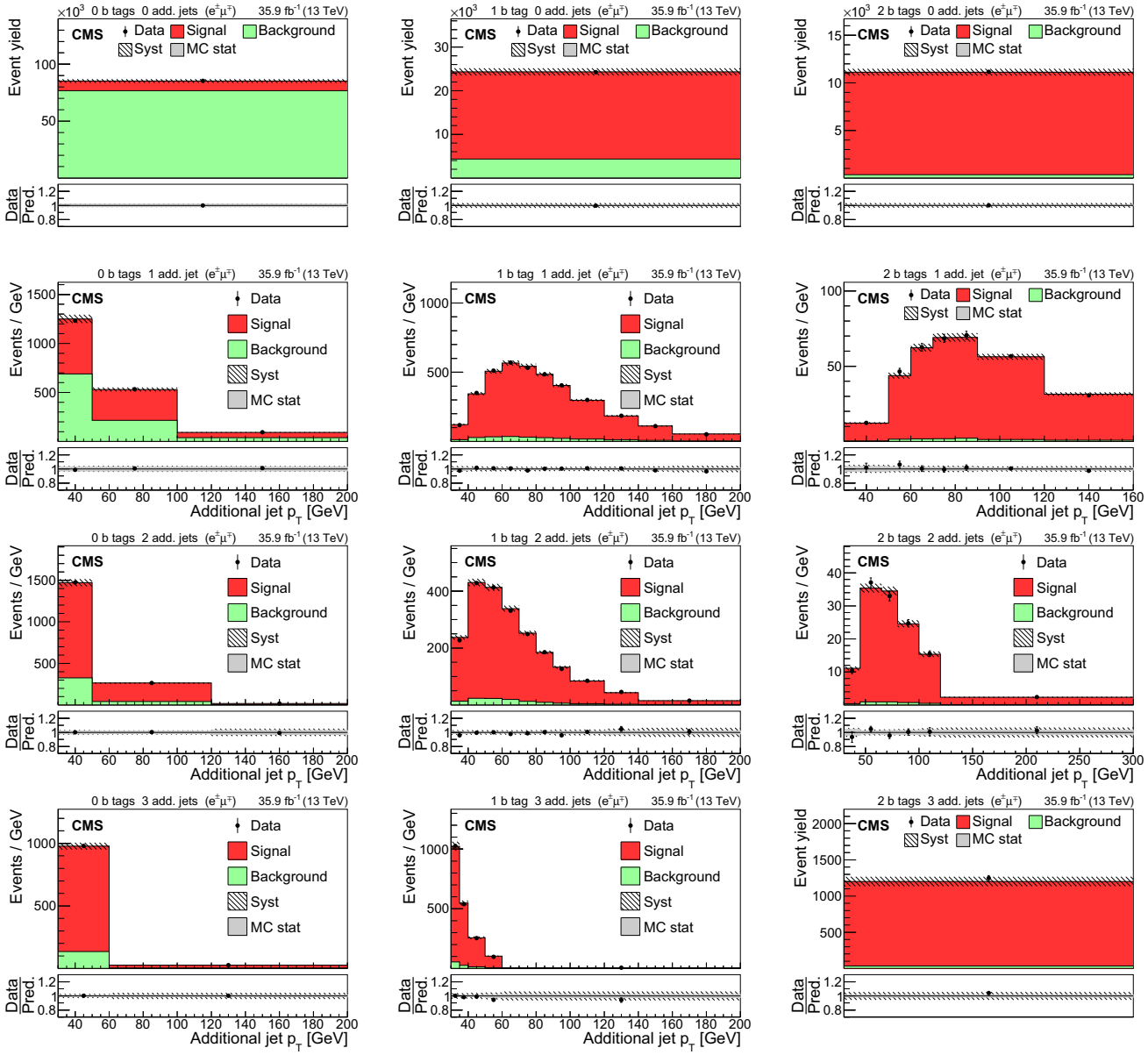

Fig. 4 Distributions in the $e^{\pm}\mu^{\mp}$ channel after the fit to the data. In the left column events with zero or three or more b-tagged jets are shown. The middle (right) column shows events with exactly one (two) b-tagged jets. Events with zero, one, two, or three or more additional non-b-tagged jets are shown in the first, second, third, and fourth row, respectively. The hatched bands correspond to the total uncertainty in the sum of the predicted yields including all correlations. The ratios of the data to the sum of the simulated yields after the fit are shown in the lower panel of each figure. Here, the solid gray band represents the contribution of the statistical uncertainty in the MC simulation

uncertainty, the simulation is used to construct template histograms that describe the expected signal and background distributions for a given nuisance parameter variation. In the fit of the templates to the data, the best values for $\sigma_{\mathrm{t\bar{t}}}^{\mathrm{vis}}$ (and $m_{\mathrm{t}}^{\mathrm{MC}}$ in the case of the combined fit) and all nuisance parameters are determined, as described in Sect. 4. The prior probability density functions for the nuisance parameters have a Gaussian shape. Table 1 shows the value of the contributions of the uncertainties after the fit.

Most of the experimental uncertainties are determined from ancillary measurements in which data and simulation are compared and small corrections to the simulation, referred to as scale factors (SFs), are determined. To assess the impact of the uncertainty in these corrections, the SFs are varied within their uncertainty and the analysis is repeated.

The trigger efficiencies are determined using multiple independent methods, which show agreement within 0.3%.

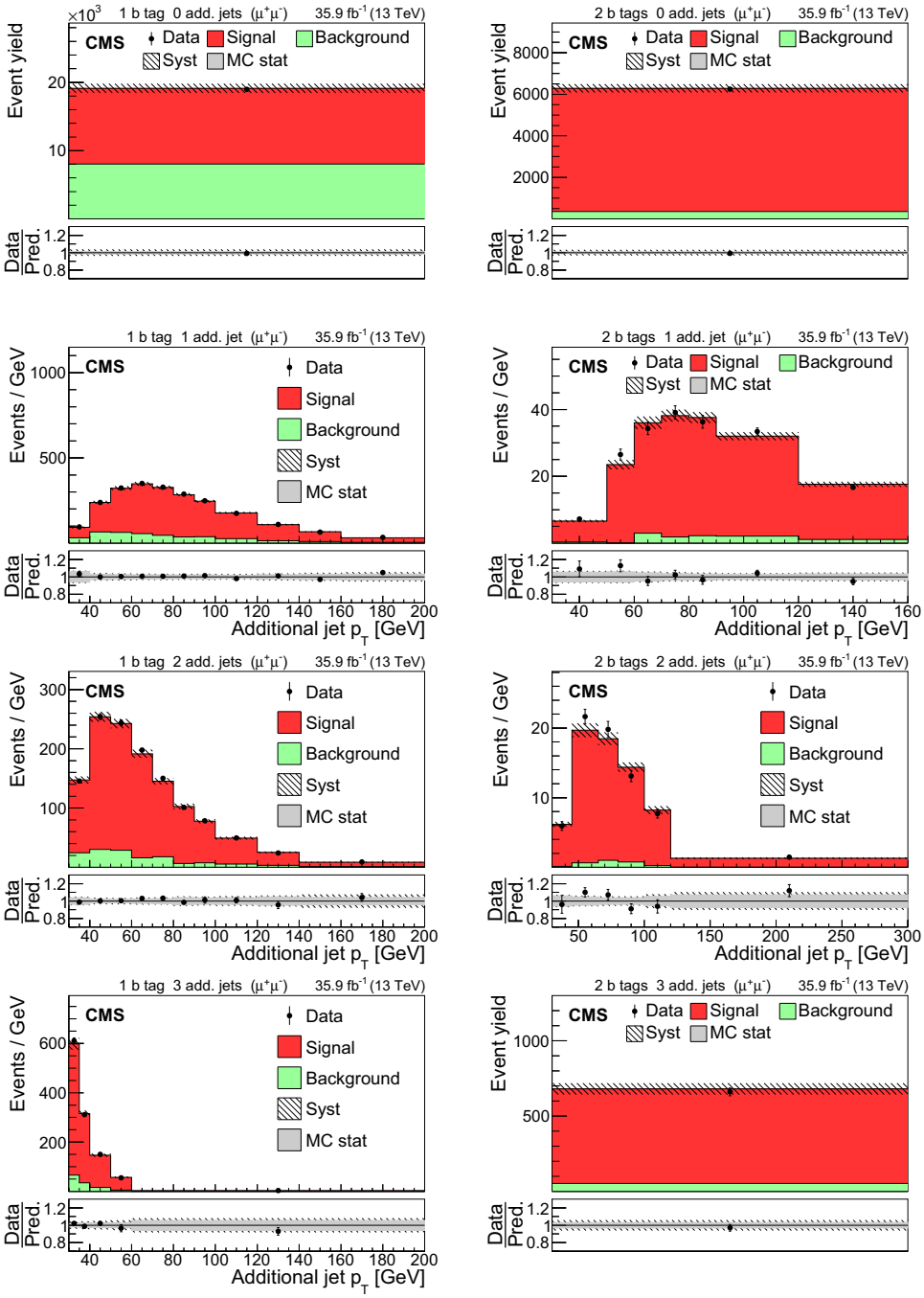

Fig. 5 Distributions in the $\mu^+\mu^-$ channel after the fit to the data. The left (right) column shows events with exactly one (two) b-tagged jets. Events with zero, one, two, or three or more additional non-b-tagged jets are shown in the first, second, third, and fourth row, respectively. The hatched bands correspond to the total uncertainty in the sum of the predicted yields including all correlations. The ratios of the data to the sum of the simulated yields after the fit are shown in the lower panel of each figure. Here, the solid gray band represents the contribution of the statistical uncertainty in the MC simulation

An additional statistical uncertainty arises because the SFs are determined from the data in intervals of p_{T} and η.

The uncertainty in the SFs of the lepton identification efficiency is typically 1.5% for electrons and 1.2% for muons, with a small dependency on the lepton p_{T} and η. The uncertainties in the calibration of the muon and electron momentum scales are included as nuisance parameters for each lepton separately. Their impact on the measurement is negligible.

The impact of the jet energy scale (JES) uncertainties is estimated by varying the jet momenta within the JES uncertainties, split into 18 contributions [59]. To account for the jet energy resolution (JER), the SFs are varied within their $|\eta|$-dependent uncertainties [62].

The uncertainties associated with the b tagging efficiency are determined by varying the related corrections for the simulation of b jets and light-flavour jets, split into 16 orthogonal contributions for b jets. These uncertainties depend on the p_{T}

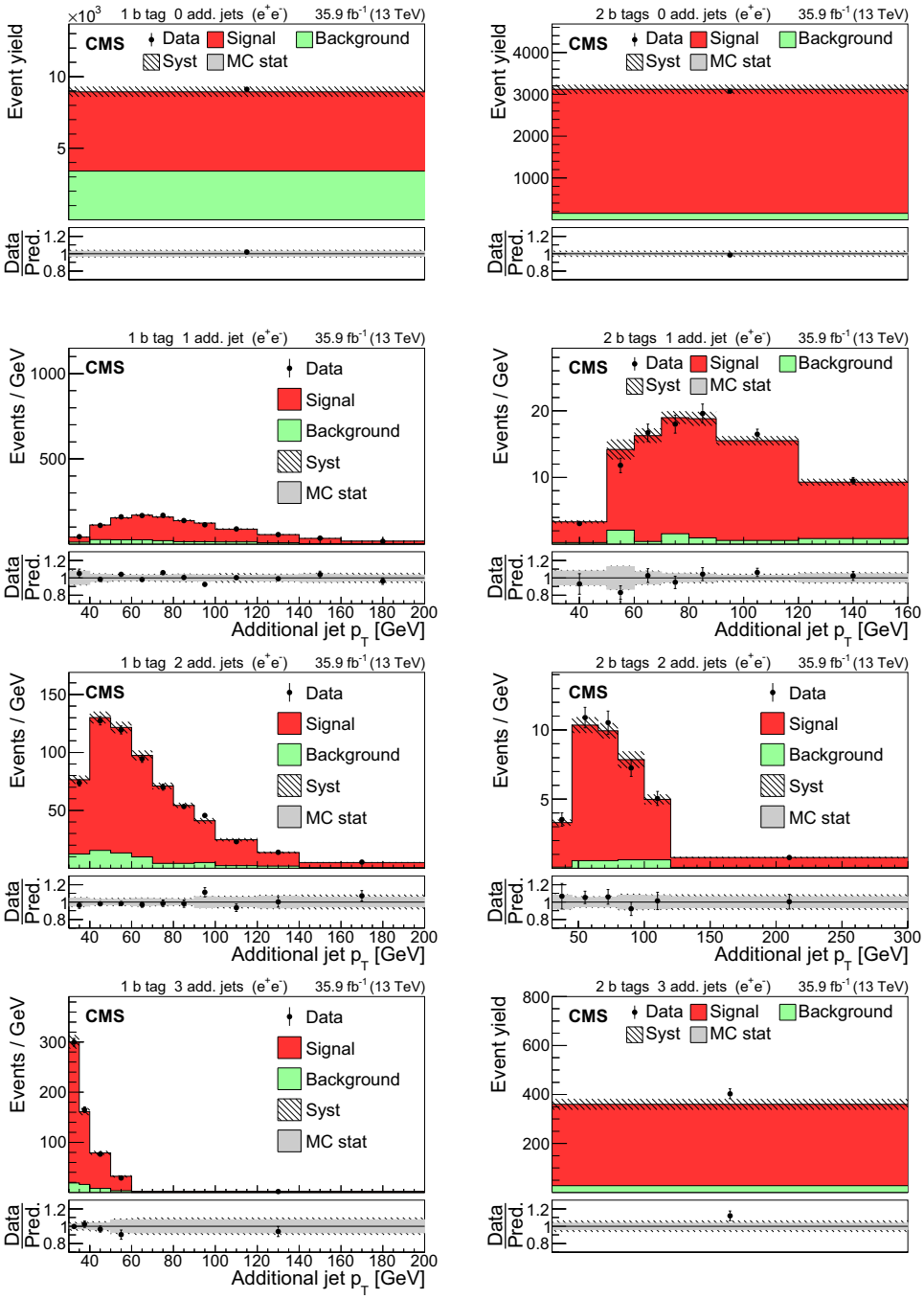

Fig. 6 Same distributions as in Fig. 5, but in the e^+e^- channel

of each jet and amount to approximately 1.5% for b jets in $t\bar{t}$ signal events [60].

The uncertainty in the modelling of the number of pileup events is obtained by changing the inelastic pp cross section, which is used to model the pileup in simulation, by $\pm$ 4.6% [48].

The integrated luminosity uncertainty is not included in the fit as a nuisance parameter, but treated as an external uncertainty. It is estimated to be 2.5% [63].

The ME scale uncertainties for the simulation of the $t\bar{t}$ and DY are assessed by varying the renormalization and factorization scale choices in POWHEG by factors of two up and down independently [64,65], avoiding cases where $\mu_f/\mu_r = 1/4$ or 4.

To estimate the uncertainty due to the NLO generator, the POWHEG $t\bar{t}$ signal sample is replaced by a $t\bar{t}$ sample generated using the MADGRAPH5_aMC@NLO program with FxFx matching [66]. This uncertainty is only included in the combined measurement of $\sigma_{t\bar{t}}$ and m_t^{MC} (Sect. 7) in order to com-

pare with the latest direct top quark mass measurement from CMS in the lepton+jets channel [31].

The PDF uncertainty is estimated using the 28 orthogonal Hessian eigenvectors of the CT14 [53] PDF, which are used as independent inputs to the fit.

Differential measurements of $\sigma_{\mathrm{t\bar{t}}}$ at $\sqrt{s} = 13\,\mathrm{TeV}$ have demonstrated that the p_{T} distribution of the top quark is softer than predicted by the POWHEG simulation [67–69]. An additional uncertainty, referred to as "Top quark p_{T}", is estimated by reweighting the simulation. This nuisance parameter has a one-sided prior distribution.

The uncertainty due to the matching of the ME to the PS in simulation is estimated by varying the h_{damp} parameter in POWHEG, as described in Ref. [40]. The uncertainty due to the assumptions in the UE tune is estimated by varying the tuning parameters [40]. The impact of the PS scale uncertainty is estimated by varying the initial-state radiation (ISR) and the final-state radiation (FSR) scales by a factor of two up and down [41], similar to the case of renormalization and factorization scales.

The uncertainties due to the assumed b hadron branching fraction (BF) and fragmentation are taken into account following the procedures described in Ref. [31]. For the fragmentation, variations of the Bowler–Lund fragmentation function [70] and the comparison to the Peterson fragmentation function [71] are considered.

The effects of colour reconnection (CR) processes on the top quark final state are estimated by enabling early resonance decays (ERD) in PYTHIA. In the nominal sample, ERD are turned off. Alternative colour reconnection models are considered, such as "gluon move" [72] and "QCD inspired" [73], since they were found to potentially have relevant effects for the measurement of the top quark mass [31].

For the uncertainties related to the background contributions, prior normalization uncertainties of 30% are assumed [74]. The contributions of these uncertainties are small and/or strongly constrained in the fit. For the DY background, separate nuisance parameters are used for each b-tagged jet category in order to remove the dependence of the fit result on the prediction of the b-tagged jet multiplicity distribution by the DY MC simulation. Similarly, the DY background is given an additional uncertainty of 5, 10, 30, and 50% for events with exactly 0, 1, 2, and 3 or more jets, respectively. The first three numbers are estimated by performing scale variations in W+jets predictions with NLO precision, whereas the last one is assigned conservatively.

In total, 103 uncertainty sources are used in the fit. In Fig. 7, the normalized pulls and constraints for the nuisance parameters related to the modelling uncertainties are shown. For each nuisance parameter, the normalized pull is defined as the difference between the best-fit and the input values, normalized to the pre-fit uncertainty, and the constraint is defined as the ratio of the post-fit to the pre-fit uncertainty. The vast

Table 1 The relative uncertainties in $\sigma_{\mathrm{t\bar{t}}}^{\mathrm{vis}}$ and $\sigma_{\mathrm{t\bar{t}}}$ and their sources, as obtained from the template fit. The uncertainty in the integrated luminosity and the MC statistical uncertainty are determined separately. The individual uncertainties are given without their correlations, which are however accounted for in the total uncertainties. Extrapolation uncertainties only affect $\sigma_{\mathrm{t\bar{t}}}$. For these uncertainties, the $\pm$ notation is used if a positive variation produces an increase in $\sigma_{\mathrm{t\bar{t}}}$, while the $\mp$ notation is used otherwise

Source	Uncertainty (%)
Trigger	0.3
Lepton ident./isolation	2.0
Muon momentum scale	0.1
Electron momentum scale	0.1
Jet energy scale	0.4
Jet energy resolution	0.4
b tagging	0.4
Pileup	0.1
$\mathrm{t\bar{t}}$ ME scale	0.2
tW ME scale	0.2
DY ME scale	0.1
PDF	1.1
Top quark p_{T}	0.5
ME/PS matching	0.2
UE tune	0.3
$\mathrm{t\bar{t}}$ ISR scale	0.4
tW ISR scale	0.1
$\mathrm{t\bar{t}}$ FSR scale	0.8
tW FSR scale	0.1
b quark fragmentation	0.7
b hadron BF	0.1
Colour reconnection	0.3
DY background	0.9
tW background	1.1
Diboson background	0.2
W+jets background	0.2
$\mathrm{t\bar{t}}$ background	0.2
Statistical	0.2
Integrated luminosity	2.5
MC statistical	1.1
Total $\sigma_{\mathrm{t\bar{t}}}^{\mathrm{vis}}$ uncertainty	3.8
Extrapolation uncertainties	
$\mathrm{t\bar{t}}$ ME scale	$\mp^{0.3}_{0.1}$
PDF	$\pm^{0.8}_{0.6}$
Top quark p_{T}	$\mp^{0.5}_{<0.1}$
$\mathrm{t\bar{t}}$ ISR scale	$\mp^{0.1}_{<0.1}$
$\mathrm{t\bar{t}}$ FSR scale	$\pm^{0.1}_{<0.1}$
UE tune	<0.1
Total $\sigma_{\mathrm{t\bar{t}}}$ uncertainty	4.0

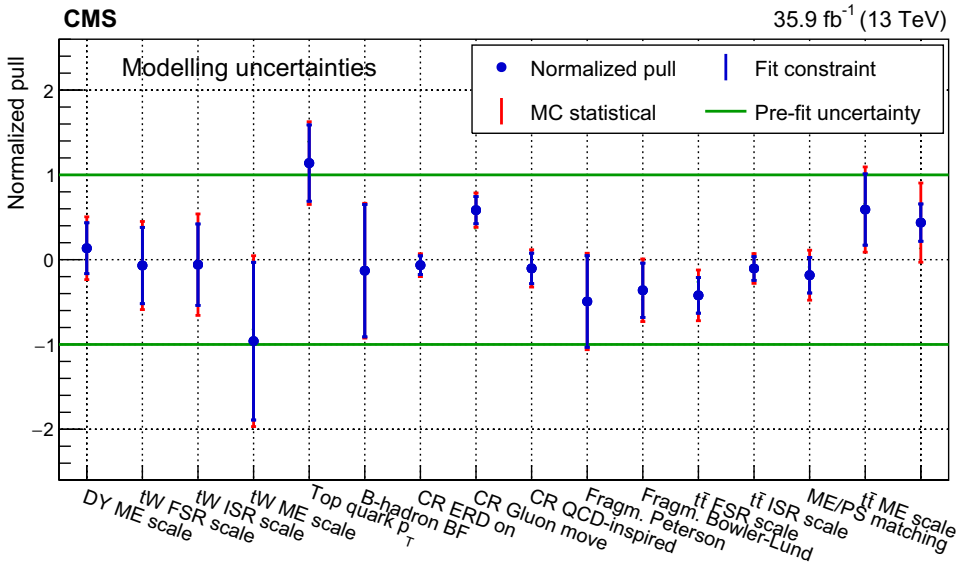

Fig. 7 Normalized pulls and constraints of the nuisance parameters related to the modelling uncertainties for the cross section fit. The markers denote the fitted values, while the inner vertical bars represent the constraint and the outer vertical bars denote the additional uncertainty as determined from pseudo-experiments. The constraint is defined as the ratio of the post-fit uncertainty to the pre-fit uncertainty of a given nuisance parameter, while the normalized pull is the difference between the post-fit and the pre-fit values of the nuisance parameter normalized to its pre-fit uncertainty. The horizontal lines at ± 1 represent the pre-fit uncertainty

majority of the nuisance parameters lie within one standard deviation of their priors, reflecting the good agreement of the nominal simulation with the data. Most $\mathrm{t\bar{t}}$ signal uncertainties show significant constraints with respect to their prior uncertainty, illustrating the strength of the analysis ansatz. The nuisance parameter for the p_{T} distribution of the top quarks is pulled by one standard deviation. This is expected since it is known that the observed p_{T} distribution of the top quark is softer than predicted by the simulation [68,69].

6 Cross section measurement

The visible cross section is defined for $\mathrm{t\bar{t}}$ events in the fiducial region with two oppositely charged leptons (electron or muon). Contributions from leptonically decaying τ leptons are included. The leading lepton is required to have $p_{\mathrm{T}} > 25\,\mathrm{GeV}$, and the subleading lepton must have $p_{\mathrm{T}} > 20\,\mathrm{GeV}$. Both leptons have to be in the range $|\eta| < 2.4$. From the likelihood fit, described in Sect. 4, the visible cross section is measured to be

$$\sigma_{\mathrm{t\bar{t}}}^{\mathrm{vis}} = 25.61 \pm 0.05\,(\mathrm{stat}) \pm 0.75\,(\mathrm{syst}) \pm 0.64\,(\mathrm{lumi})\,\mathrm{pb}.$$

Here, the uncertainties denote the statistical uncertainty, the systematic uncertainty, and that coming from the uncertainty in the integrated luminosity. The full list of uncertainties is presented in Table 1.

The total cross section $\sigma_{\mathrm{t\bar{t}}}$ is obtained by extrapolating the measured visible cross section to the full phase space. As explained in Sect. 4, the extrapolation is described by a multiplicative acceptance correction factor $A_{\ell\ell}$ (see Eq. (1)). The extrapolation uncertainty is determined for each relevant model systematic source j as described in the following: all nuisance parameters except the one under study are fixed to their post-fit values; the nuisance parameter λ_j is set to values $+1$ and -1, and the variations of $A_{\ell\ell}$ are recorded. The resulting variations of $\sigma_{\mathrm{t\bar{t}}}$ with respect to the nominal value, obtained with the post-fit value of λ_j, are taken as the additional extrapolation uncertainties. The individual uncertainties in $\sigma_{\mathrm{t\bar{t}}}$ from these sources are summed in quadrature to estimate the total systematic uncertainty, as summarized in Table 1. A fixed value of $m_{\mathrm{t}}^{\mathrm{MC}} = 172.5\,\mathrm{GeV}$ is chosen in the simulation, and no uncertainty is assigned.

The total cross section $\sigma_{\mathrm{t\bar{t}}}$ is measured to be

$$\sigma_{\mathrm{t\bar{t}}} = 803 \pm 2\,(\mathrm{stat}) \pm 25\,(\mathrm{syst}) \pm 20\,(\mathrm{lumi})\,\mathrm{pb}.$$

As shown in Table 1, in comparison to the fiducial cross section, the relative systematic uncertainty in the total cross section is marginally increased. The result is in good agreement with the theoretical calculation at NNLO+NNLL, which predicts a $\mathrm{t\bar{t}}$ cross section of $832\,^{+20}_{-29}\,(\mathrm{scale}) \pm 35\,(\mathrm{PDF}+\alpha_S)\,\mathrm{pb}$, as described in Sect. 2.

An independent cross section measurement is performed using a simple event-counting method and a more restrictive event selection, following closely the analysis of Ref. [75].

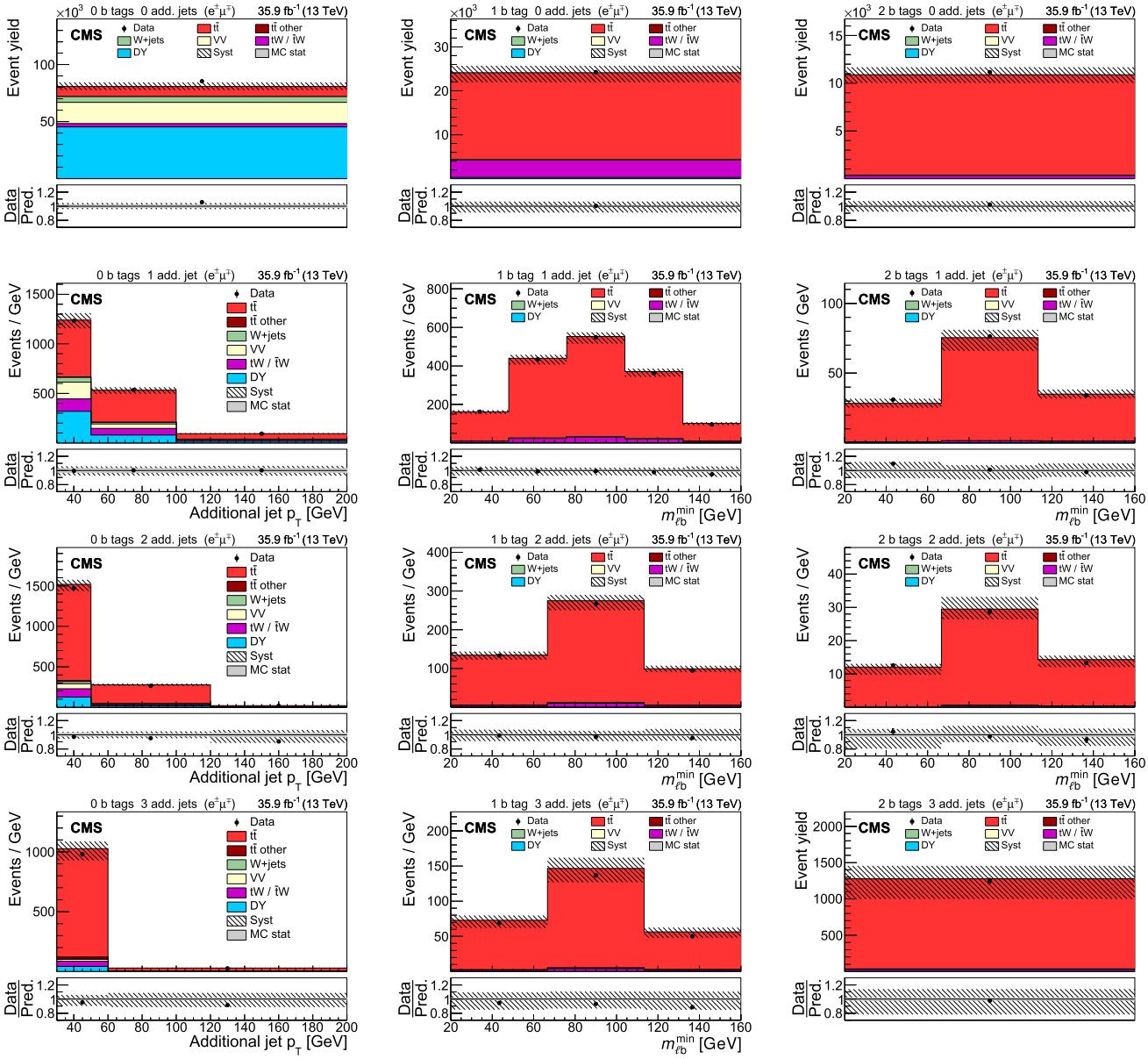

Fig. 8 Comparison of data (points) and pre-fit distributions of the expected signal and backgrounds from simulation (shaded histograms) used in the simultaneous fit of $\sigma_{\mathrm{t\bar{t}}}$ and $m_{\mathrm{t}}^{\mathrm{MC}}$ in the $\mathrm{e}^{\pm}\mu^{\mp}$ channel. In the left column events with zero or three or more b-tagged jets are shown. The middle (right) column shows events with exactly one (two) b-tagged jets. Events with zero, one, two, or three or more additional non-b-tagged jets are shown in the first, second, third, and fourth row, respectively. The hatched bands correspond to the total uncertainty in the sum of the predicted yields. The ratios of data to the sum of the predicted yields are shown in the lower panel of each figure. Here, the solid gray band represents the contribution of the statistical uncertainty

The analysis uses events in the $\mathrm{e}^{\pm}\mu^{\mp}$ channel with at least two jets, at least one of which is b tagged. The cross section is measured to be $\sigma_{\mathrm{t\bar{t}}} = 804 \pm 2\,(\mathrm{stat}) \pm 31\,(\mathrm{syst}) \pm 20\,(\mathrm{lumi})$ pb, in good agreement with the main result.

7 Simultaneous measurement of $\sigma_{\mathrm{t\bar{t}}}$ and $m_{\mathrm{t}}^{\mathrm{MC}}$

The analysis is designed such that the dependence of the measured $\mathrm{t\bar{t}}$ cross section on $m_{\mathrm{t}}^{\mathrm{MC}}$ is small. However, because of the impact of the top quark mass on the simulated detector efficiency and acceptance, the measurement is expected to have a residual dependence on the chosen value of $m_{\mathrm{t}}^{\mathrm{MC}}$. In previous measurements, this dependence was determined by repeating the analysis with varied mass values.

Here, the approach proposed in Refs. [5,30] is followed. The value of $m_{\mathrm{t}}^{\mathrm{MC}}$ is introduced in the fit as an additional free parameter. In the simultaneous fit, $\sigma_{\mathrm{t\bar{t}}}$ and $m_{\mathrm{t}}^{\mathrm{MC}}$ are directly constrained from the data. The resulting $\sigma_{\mathrm{t\bar{t}}}$ and its uncer-

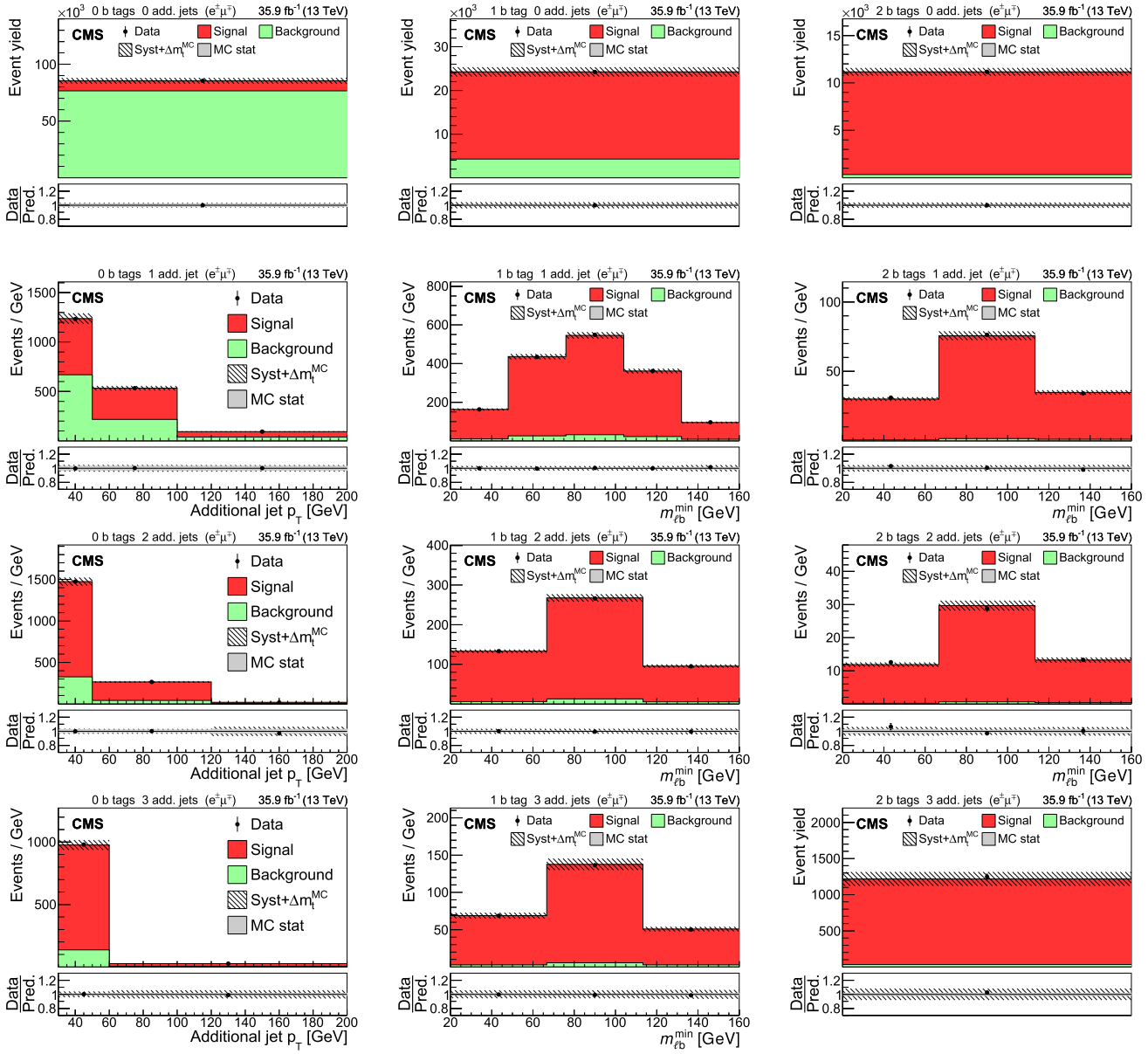

Fig. 9 Comparison of data (points) and post-fit distributions of the expected signal and backgrounds from simulation (shaded histograms) used in the simultaneous fit of $\sigma_{\mathrm{t\bar{t}}}$ and $m_{\mathrm{t}}^{\mathrm{MC}}$ in the $\mathrm{e}^{\pm}\mu^{\mp}$ channel. In the left column events with zero or three or more b-tagged jets are shown. The middle (right) column shows events with exactly one (two) b-tagged jets. Events with zero, one, two, or three or more additional non-b-tagged jets are shown in the first, second, third, and fourth row, respectively. The hatched bands correspond to the total uncertainty in the sum of the predicted yields and include the contribution from the top quark mass ($\Delta m_{\mathrm{t}}^{\mathrm{MC}}$). The ratios of data to the sum of the predicted yields are shown in the lower panel of each figure. Here, the solid gray band represents the contribution of the statistical uncertainty

tainty therefore account for the dependence on $m_{\mathrm{t}}^{\mathrm{MC}}$ and can be used, e.g. for the extraction of m_{t} and α_S using fixed-order calculations. The value of $m_{\mathrm{t}}^{\mathrm{MC}}$, in turn, can be compared to the results of direct measurements using, e.g. kinematic fits [31].

In contrast to the $\sigma_{\mathrm{t\bar{t}}}$ measurement presented in Sect. 6, the sensitivity of the simultaneous fit to $m_{\mathrm{t}}^{\mathrm{MC}}$ is maximized by introducing a new observable: the minimum invariant mass $m_{\ell\mathrm{b}}^{\mathrm{min}}$, which is defined as the smallest invariant mass found when combining the charged leptons with the b jets in an event. To minimize the impact from background, only the $\mathrm{e}^{\pm}\mu^{\mp}$ sample is used. The simultaneous fit of $\sigma_{\mathrm{t\bar{t}}}$ and $m_{\mathrm{t}}^{\mathrm{MC}}$ is performed in 12 mutually exclusive categories, according to the number of b-tagged jets and of additional non-b-tagged jets in the event. The same observables as in Fig. 4 are used as input to the fit, where the jet p_{T} spectrum is replaced by

Table 2 The same as Table 1, but for the simultaneous fit of $\sigma_{t\bar{t}}$ and m_t^{MC}

Source	Uncertainty (%)
Trigger	0.4
Lepton ident./isolation	2.2
Muon momentum scale	0.2
Electron momentum scale	0.2
Jet energy scale	0.7
Jet energy resolution	0.5
b tagging	0.3
Pileup	0.3
$t\bar{t}$ ME scale	0.5
tW ME scale	0.7
DY ME scale	0.2
NLO generator	1.2
PDF	1.1
m_t^{MC}	0.4
Top quark p_T	0.5
ME/PS matching	0.2
UE tune	0.3
$t\bar{t}$ ISR scale	0.4
tW ISR scale	0.4
$t\bar{t}$ FSR scale	1.1
tW FSR scale	0.2
b quark fragmentation	1.0
b hadron BF	0.2
Colour reconnection	0.4
DY background	0.8
tW background	1.1
Diboson background	0.3
W+jets background	0.3
$t\bar{t}$ background	0.2
Statistical	0.2
Integrated luminosity	2.5
MC statistical	1.2
Total $\sigma_{t\bar{t}}^{vis}$ uncertainty	4.2
Extrapolation uncertainties	
$t\bar{t}$ ME scale	$\mp^{0.4}_{<0.1}$
PDF	$\pm^{0.8}_{0.6}$
Top quark p_T	$\pm^{0.2}_{0.3}$
$t\bar{t}$ ISR scale	$\mp^{0.2}_{<0.1}$
$t\bar{t}$ FSR scale	± 0.1
UE tune	<0.1
m_t^{MC}	$\mp^{0.2}_{0.3}$
Total $\sigma_{t\bar{t}}$ uncertainty	$^{+4.3}_{-4.2}$

the $m_{\ell b}^{min}$ distribution in categories with at least one b-tagged jet, as shown in Fig. 8.

Table 3 The absolute uncertainties in m_t^{MC} and their sources, from the simultaneous fit of $\sigma_{t\bar{t}}$ and m_t^{MC}. The MC statistical uncertainty is determined separately. The individual uncertainties are given without their correlations, which are however accounted for in the total uncertainties

Source	Uncertainty (GeV)
Trigger	0.02
Lepton ident./isolation	0.02
Muon momentum scale	0.03
Electron momentum scale	0.10
Jet energy scale	0.57
Jet energy resolution	0.09
b tagging	0.12
Pileup	0.09
$t\bar{t}$ ME scale	0.18
tW ME scale	0.02
DY ME scale	0.06
NLO generator	0.14
PDF	0.05
$\sigma_{t\bar{t}}$	0.09
Top quark p_T	0.04
ME/PS matching	0.16
UE tune	0.03
$t\bar{t}$ ISR scale	0.16
tW ISR scale	0.02
$t\bar{t}$ FSR scale	0.07
tW FSR scale	0.02
b quark fragmentation	0.11
b hadron BF	0.07
Colour reconnection	0.17
DY background	0.24
tW background	0.13
Diboson background	0.02
W+jets background	0.04
$t\bar{t}$ background	0.02
Statistical	0.14
MC statistical	0.36
Total m_t^{MC} uncertainty	$^{+0.68}_{-0.73}$

To construct the templates describing the dependence of the final-state distributions on m_t^{MC}, separate MC simulation samples of $t\bar{t}$ and tW production are used in which m_t^{MC} is varied in the range $m_t^{MC} = 172.5 \pm 3$ GeV. The data and MC samples, the event selection, the modelling of the systematic uncertainties, and the fit procedure are identical to those described in Sect. 4. In the simultaneous fit, the same systematic uncertainties are included as in a previous CMS measurement [31] of the m_t^{MC}. The results of the two measurements are thus directly comparable.

Comparisons of the data and the prediction from the MC simulation before and after the fit are presented in Figs. 8 and 9, respectively. Good agreement is found in both cases.

The result of the fit is found to be stable against the choice of the fit distributions, and the introduction of the $m_{\ell b}^{\min}$ distribution was confirmed not to alter the final result on $\sigma_{t\bar{t}}$ or the behaviour with respect to the nuisance parameters. The procedure is calibrated by performing fits where data is replaced by simulations with different m_t^{MC} hypotheses: full closure of the method is obtained and no additional correction is applied. The effect of the statistical uncertainty in the simulation on the fit results is estimated as explained in Sect. 4 and is considered as an additional uncertainty. The results for $\sigma_{t\bar{t}}$ and m_t^{MC} are

$$\sigma_{t\bar{t}} = 815 \pm 2\,(\text{stat}) \pm 29\,(\text{syst}) \pm 20\,(\text{lumi})\,\text{pb},$$
$$m_t^{MC} = 172.33 \pm 0.14\,(\text{stat})\,^{+0.66}_{-0.72}\,(\text{syst})\,\text{GeV}.$$

The value for the cross section is in good agreement with the result obtained for a fixed value of $m_t^{MC} = 172.5\,\text{GeV}$, reported in Sect. 6. The correlation between the two parameters is found to be 12%.

The results of the simultaneous fit to $\sigma_{t\bar{t}}$ and m_t^{MC} are summarized in Tables 2 and 3, respectively, together with the contribution of each systematic uncertainty to the total uncertainty. Normalized pulls and constraints of the nuisance parameters related to modelling uncertainties are shown in Fig. 10. The nuisance parameters displayed in this figure show similar trends to those in Fig. 7, described above. Here, the constraints on the nuisance parameters tend to be less stringent because only data in the $e^{\pm}\mu^{\mp}$ channel are used to determine the two parameters of interest, using mostly the $m_{\ell b}^{\min}$ spectra in place of the jet p_T distributions within the jet and b-tagged jet categories.

As a cross-check, a measurement of m_t^{MC} is performed by fitting a single $m_{\ell b}^{\min}$ distribution containing all events with at least one b-tagged jet. The resulting value is $m_t^{MC} = 171.92 \pm 0.13\,(\text{stat})\,^{+0.76}_{-0.77}\,(\text{syst})\,\text{GeV}$. Since the uncorrelated uncertainty with respect to the main result is estimated to be at least 0.54 GeV, which is larger than the difference between the two measurements, the two results are in good agreement.

8 Extraction of m_t and $\alpha_S(m_Z)$ in the $\overline{\text{MS}}$ scheme

The cross section value obtained in the simultaneous fit to $\sigma_{t\bar{t}}$ and m_t^{MC} is used to extract $\alpha_S(m_Z)$ and m_t in the $\overline{\text{MS}}$ renormalization scheme. For this purpose, the measured and the predicted cross sections are compared via a χ^2 minimization. The χ^2 fit is performed using the open-source QCD analysis framework xFitter [76] and a χ^2 definition from Ref. [77]. The method to determine m_t and $\alpha_S(m_Z)$ is very similar to the one used in earlier CMS analyses to extract $\alpha_S(m_Z)$ using jet cross section measurements, e.g. in Ref. [78].

It is assumed that the measured $\sigma_{t\bar{t}}$ is not affected by non-SM physics. The SM theoretical prediction for $\sigma_{t\bar{t}}$ at NNLO [6–9] is calculated using the Hathor 2.0 [79] program, interfaced with xFitter. This is the only available calculation to date that provides the m_t definition in the $\overline{\text{MS}}$ scheme. The top quark mass in the $\overline{\text{MS}}$ scheme is denoted by $m_t(m_t)$, following the convention of presenting the value of a running coupling at a fixed value. In the calculation, the renormalization and factorization scales, μ_r and μ_f, are set to $m_t(m_t)$. These are varied by a factor of two up and down, independently, avoiding cases where μ_f/μ_r = 1/4 or 4, in order to estimate the uncertainty due to the missing higher-order corrections (referred to in the following as the scale variation uncertainty).

The values of $\alpha_S(m_Z)$ and m_t cannot be determined simultaneously, since both parameters alter the predicted $\sigma_{t\bar{t}}$ in such a way that any variation of one parameter can be compensated by a variation of the other. In the presented analysis, the values of m_t and $\alpha_S(m_Z)$ are therefore determined at fixed values of $\alpha_S(m_Z)$ and m_t, respectively.

The four most recent PDF sets available [80] at NNLO are used:ABMP16nnlo [17],CT14nnlo [53], MMHT14nnlo [81], and NNPDF3.1nnlo [82]. While CT14nnlo does not use any $t\bar{t}$ data as input, the PDF sets ABMP16nnlo and MMHT14nnlo use measurements of inclusive $t\bar{t}$ cross sections at the Tevatron and LHC, and NNPDF3.1nnlo makes use of all available inclusive and differential $t\bar{t}$ cross section measurements. Using the currently available $t\bar{t}$ measurements has only a marginal effect on a global PDF and $\alpha_S(m_Z)$ fit [17,53]. The details of the PDFs relevant for this analysis are summarized in Table 4. In the MMHT14nnlo, CT14nnlo, and NNPDF3.1nnlo PDFs, the value of $\alpha_S(m_Z)$ is assumed to be 0.118. In ABMP16nnlo, $\alpha_S(m_Z)$ is fitted simultaneously with the PDFs. The ABMP16nnlo PDF employs the $\overline{\text{MS}}$ scheme for the heavy-quark mass treatment in its determination. Similar to the value of $\alpha_S(m_Z)$, the value of $m_t(m_t)$ in the ABMP16nnlo set is obtained in a simultaneous fit with the PDFs. For the other PDFs, the values of m_t^{pole} are assumed, as listed in Table 4. Since the analysis is performed in the $\overline{\text{MS}}$ scheme, the assumed m_t^{pole} of each PDF is converted into $m_t(m_t)$ using the RunDec [83,84] code, according to the prescription by the corresponding PDF group.

For each used PDF set, a series of $\alpha_S(m_Z)$ values is provided. The PDF uncertainties for all sets correspond to a 68% confidence level (CL), whereby the uncertainties in the CT14nnlo PDF set are scaled down from 95% CL.

Because of the strong correlation between α_S and m_t in the prediction of $\sigma_{t\bar{t}}$, for the m_t extraction, the value of $\alpha_S(m_Z)$ in the theoretical prediction is set to that of the particular PDF

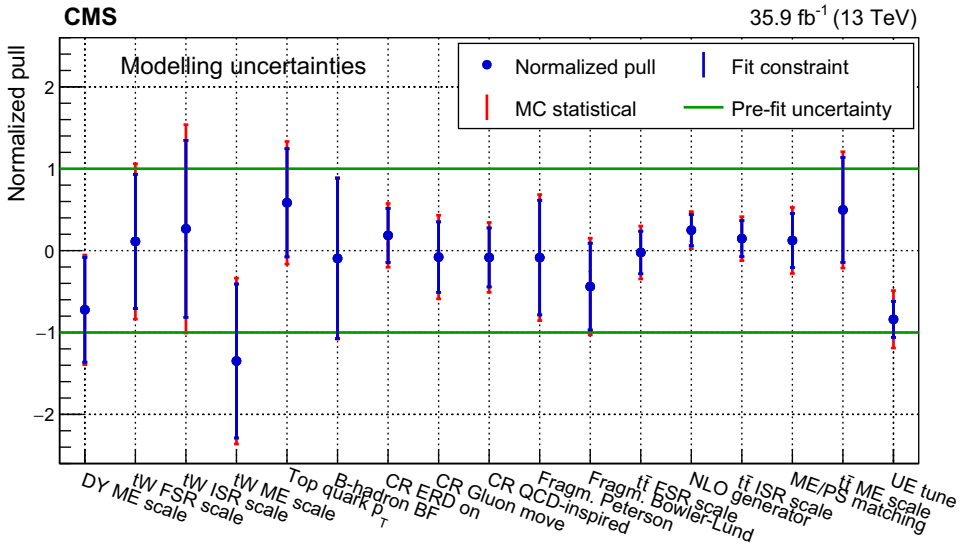

Fig. 10 Normalized pulls and constraints of the nuisance parameters related to the modelling uncertainties for the simultaneous fit of $\sigma_{\mathrm{t\bar{t}}}$ and $m_{\mathrm{t}}^{\mathrm{MC}}$. The markers denote the fitted value, while the inner vertical bars represent the constraint and the outer vertical bars denote the additional uncertainty as determined from pseudo-experiments. The constraint is defined as the ratio of the post-fit uncertainty to the pre-fit uncertainty of a given nuisance parameter, while the normalized pull is the difference between the post-fit and the pre-fit values of the nuisance parameter normalized to its pre-fit uncertainty. The horizontal lines at $\pm$ 1 represent the pre-fit uncertainty

Table 4 Values of the top quark pole mass $m_{\mathrm{t}}^{\mathrm{pole}}$ and strong coupling constant $\alpha_S(m_{\mathrm{Z}})$ used in the different PDF sets. Also shown are the corresponding $m_{\mathrm{t}}(m_{\mathrm{t}})$ values obtained using the RunDec [83,84] conversion, the number of loops in the conversion, and the α_S range used to estimate the PDF uncertainties

	ABMP16	NNPDF3.1	CT14	MMHT14
$m_{\mathrm{t}}^{\mathrm{pole}}$ [GeV]	170.37	172.5	173.3	174.2
RunDec loops	3	2	2	3
$m_{\mathrm{t}}(m_{\mathrm{t}})$ [GeV]	160.86	162.56	163.30	163.47
$\alpha_S(m_{\mathrm{Z}})$	0.116	0.118	0.118	0.118
α_S range	0.112–0.120	0.108–0.124	0.111–0.123	0.108–0.128

set. Similarly, in the theoretical prediction of $\sigma_{\mathrm{t\bar{t}}}$ used for the $\alpha_S(m_{\mathrm{Z}})$ determination, the value of m_{t} is the one used in the PDF evaluation. The correlation of the values of $m_{\mathrm{t}}(m_{\mathrm{t}})$, $\alpha_S(m_{\mathrm{Z}})$, and the proton PDFs in the prediction of $\sigma_{\mathrm{t\bar{t}}}$ is also studied.

To extract the value of $\alpha_S(m_{\mathrm{Z}})$ from $\sigma_{\mathrm{t\bar{t}}}$, the measured cross section is compared to the theoretical prediction, and for each $\alpha_S(m_{\mathrm{Z}})$ member of each PDF set, the χ^2 is evaluated. In the case of ABMP16nnlo and NNPDF3.1nnlo, the complete set of PDF uncertainties is provided for each member of the $\alpha_S(m_{\mathrm{Z}})$ series and is accounted for in the analysis. The uncertainties in the CT14nnlo and MMHT14nnlo PDFs are evaluated only for the central $\alpha_S(m_{\mathrm{Z}})$ value of 0.118 and are used for each $\alpha_S(m_{\mathrm{Z}})$ variant in the fit. The optimal value of $\alpha_S(m_{\mathrm{Z}})$ is subsequently determined from a parabolic fit of the form

$$\chi^2(\alpha_S) = \chi^2_{\mathrm{min}} + \left(\frac{\alpha_S - \alpha_S^{\mathrm{min}}}{\delta(\alpha_S^{\mathrm{min}})} \right)^2 \quad (7)$$

to the $\chi^2(\alpha_S)$ values. Here, χ^2_{min} is the χ^2 value at $\alpha_S = \alpha_S^{\mathrm{min}}$ and $\delta(\alpha_S^{\mathrm{min}})$ is the fitted experimental uncertainty in α_S^{min}, which also accounts for the PDF uncertainty. The $\chi^2(\alpha_S)$ scan is illustrated in Fig. 11 for the PDF sets used, demonstrating a clear parabolic behaviour. To estimate the scale variation uncertainties, this procedure is repeated with μ_{r} and μ_{f} being varied, and the largest deviations of the resulting values of α_S^{min} from that of the central scale choice are considered as the corresponding uncertainties. The values of the $\alpha_S(m_{\mathrm{Z}})$ obtained using different PDFs are listed in Table 5 and shown in Fig. 11. The uncertainties in the measured $\sigma_{\mathrm{t\bar{t}}}$ and the PDF contribute about equally to the resulting $\alpha_S(m_{\mathrm{Z}})$ uncertainty.

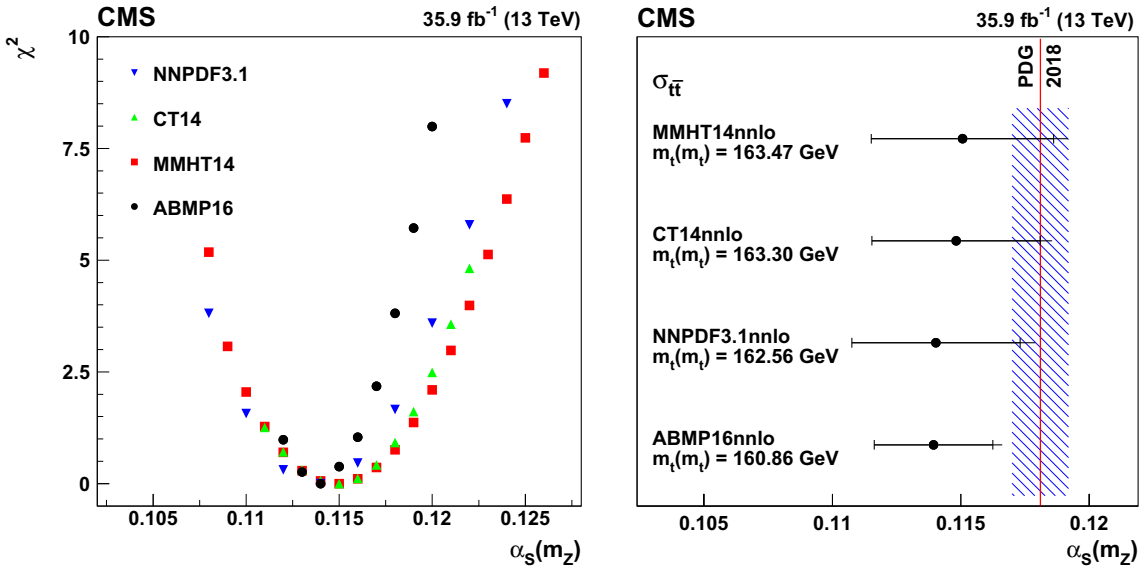

Fig. 11 Left: χ^2 versus α_S obtained from the comparison of the measured $\sigma_{\mathrm{t\bar{t}}}$ value to the NNLO prediction in the $\overline{\mathrm{MS}}$ scheme using different PDFs (symbols of different styles). Right: $\alpha_S(m_Z)$ obtained from the comparison of the measured $\sigma_{\mathrm{t\bar{t}}}$ value to the theoretical prediction using different PDF sets in the $\overline{\mathrm{MS}}$ scheme. The corresponding value of $m_{\mathrm{t}}(m_{\mathrm{t}})$ is given for each PDF set. The inner horizontal bars on the points represent the experimental and PDF uncertainties added in quadrature. The outer horizontal bars show the total uncertainties. The vertical line displays the world-average $\alpha_S(m_Z)$ value [29], with the hatched band representing its uncertainty

Table 5 Values of $\alpha_S(m_Z)$ with their uncertainties obtained from a comparison of the measured $\sigma_{\mathrm{t\bar{t}}}$ value to the NNLO prediction in the $\overline{\mathrm{MS}}$ scheme using different PDF sets. The first uncertainty is the combination of the experimental and PDF uncertainties, and the second is from the variation of the renormalization and factorization scales

PDF set	$\alpha_S(m_Z)$
ABMP16	0.1139 ± 0.0023 (fit + PDF) $^{+0.0014}_{-0.0001}$ (scale)
NNPDF3.1	0.1140 ± 0.0033 (fit + PDF) $^{+0.0021}_{-0.0002}$ (scale)
CT14	0.1148 ± 0.0032 (fit + PDF) $^{+0.0018}_{-0.0002}$ (scale)
MMHT14	0.1151 ± 0.0035 (fit + PDF) $^{+0.0020}_{-0.0002}$ (scale)

Table 6 Values of $m_{\mathrm{t}}(m_{\mathrm{t}})$ obtained from the comparison of the $\sigma_{\mathrm{t\bar{t}}}$ measurement with the NNLO predictions using different PDF sets. The first uncertainty shown comes from the experimental, PDF, and $\alpha_S(m_Z)$ uncertainties, and the second from the variation in the renormalization and factorization scales

PDF set	$m_{\mathrm{t}}(m_{\mathrm{t}})$ (GeV)
ABMP16	161.6 ± 1.6 (fit + PDF + α_S) $^{+0.1}_{-1.0}$ (scale)
NNPDF3.1	164.5 ± 1.6 (fit + PDF + α_S) $^{+0.1}_{-1.0}$ (scale)
CT14	165.0 ± 1.8 (fit + PDF + α_S) $^{+0.1}_{-1.0}$ (scale)
MMHT14	164.9 ± 1.8 (fit + PDF + α_S) $^{+0.1}_{-1.1}$ (scale)

The values of $\alpha_S(m_Z)$ obtained using different PDF sets are consistent among each other and are in agreement with the world-average value [29] within the uncertainties, although suggesting a smaller value of $\alpha_S(m_Z)$. The value of $\alpha_S(m_Z)$ is also in good agreement with the recent result of the analysis in Ref. [85] of jet production in deep-inelastic scattering using the NNLO calculation by the H1 experiment, and is of comparable precision.

The same procedure is used to extract $m_{\mathrm{t}}(m_{\mathrm{t}})$ by fixing $\alpha_S(m_Z)$ to the nominal value at which the used PDF is evaluated. The fit is performed by varying $m_{\mathrm{t}}(m_{\mathrm{t}})$ in a 5-GeV range around the central value used in each PDF. The uncertainties related to the variation of $\alpha_S(m_Z)$ in the PDF are estimated by repeating the fit using the PDF eigenvectors with $\alpha_S(m_Z)$ varied within its uncertainty, as provided by NNPDF3.1nnlo, MMHT2014nnlo, and CT14nnlo. In the case of ABMP16nnlo, the value of $\alpha_S(m_Z)$ is a free parameter in the PDF fit and its uncertainty is implicitly included in the ABMP16nnlo PDF uncertainty eigenvectors. The resulting $m_{\mathrm{t}}(m_{\mathrm{t}})$ values are summarized in Table 6, where the fit uncertainty corresponds to the precision of the $\sigma_{\mathrm{t\bar{t}}}$ measurement. The results obtained with different PDF sets are in agreement, although the ABMP16nnlo PDF set yields a systematically lower value. This difference is expected and has its origin in a larger value of $\alpha_S(m_Z) = 0.118$ assumed in the NNPDF3.1, MMHT2014, and CT14 PDFs.

The values of $m_{\mathrm{t}}(m_{\mathrm{t}})$ are in agreement with those originally used in the evaluation of each PDF set. The results are shown in Fig. 12 for the four different PDFs used.

The dependence of the $\alpha_S(m_Z)$ result on the assumption on $m_{\mathrm{t}}(m_{\mathrm{t}})$ is investigated for each PDF by performing the $\chi^2(\alpha_S)$ scan for ten values of $m_{\mathrm{t}}(m_{\mathrm{t}})$ varying from 160.5

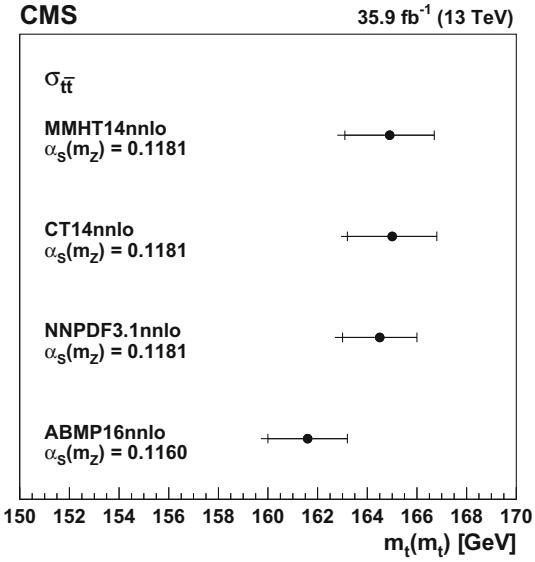

Fig. 12 Values of $m_{\mathrm{t}}(m_{\mathrm{t}})$ obtained from comparing the $\sigma_{\mathrm{t\bar{t}}}$ measurement to the theoretical NNLO predictions using different PDF sets. The inner horizontal bars on the points represent the quadratic sum of the experimental, PDF, and $\alpha_S(m_Z)$ uncertainties, while the outer horizontal bars give the total uncertainties

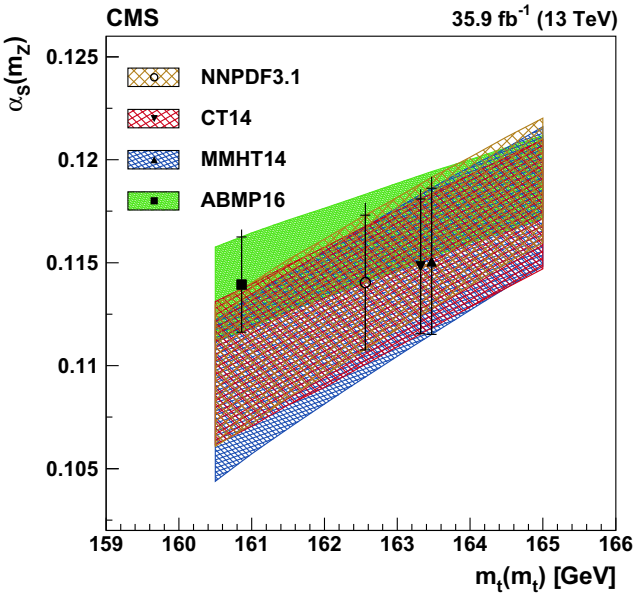

Fig. 13 Values of $\alpha_S(m_Z)$ obtained in the comparison of the $\sigma_{\mathrm{t\bar{t}}}$ measurement to the NNLO prediction using different PDFs, as a function of the $m_{\mathrm{t}}(m_{\mathrm{t}})$ value used in the theoretical calculation. The results from using the different PDFs are shown by the bands with different shadings, with the band width corresponding to the quadratic sum of the experimental and PDF uncertainties in $\alpha_S(m_Z)$. The resulting measured values of $\alpha_S(m_Z)$ are shown by the different style points at the $m_{\mathrm{t}}(m_{\mathrm{t}})$ values used for each PDF. The inner vertical bars on the points represent the quadratic sum of the experimental and PDF uncertainties in $\alpha_S(m_Z)$, while the outer vertical bars show the total uncertainties

Table 7 Values of $m_{\mathrm{t}}^{\mathrm{pole}}$ obtained by comparing the $\sigma_{\mathrm{t\bar{t}}}$ measurement with predictions at NNLO+NNLL using different PDF sets

PDF set	$m_{\mathrm{t}}^{\mathrm{pole}}$ (GeV)
ABMP16	$169.9 \pm 1.8\,(\mathrm{fit} + \mathrm{PDF} + \alpha_S)\,^{+0.8}_{-1.2}\,(\mathrm{scale})$
NNPDF3.1	$173.2 \pm 1.9\,(\mathrm{fit} + \mathrm{PDF} + \alpha_S)\,^{+0.9}_{-1.3}\,(\mathrm{scale})$
CT14	$173.7 \pm 2.0\,(\mathrm{fit} + \mathrm{PDF} + \alpha_S)\,^{+0.9}_{-1.4}\,(\mathrm{scale})$
MMHT14	$173.6 \pm 1.9\,(\mathrm{fit} + \mathrm{PDF} + \alpha_S)\,^{+0.9}_{-1.4}\,(\mathrm{scale})$

to 165.0 GeV. A linear dependence is observed, as shown in Fig. 13.

9 Extraction of m_{t} in the pole mass scheme

The extraction of m_{t} is repeated in the pole mass scheme using the Top++ 2.0 program [52], which employs the calculation of $\sigma_{\mathrm{t\bar{t}}}$ at NNLO, improved by the NNLL soft-gluon resummation. The results are summarized in Table 7. The scale variation uncertainties are estimated in the same way as in the case of the $m_{\mathrm{t}}(m_{\mathrm{t}})$ extraction. These uncertainties are larger than those determined in the $\overline{\mathrm{MS}}$ scheme. This is because of the better convergence of the perturbative series when using the $\overline{\mathrm{MS}}$ renormalization scheme in the calculation of $\sigma_{\mathrm{t\bar{t}}}$.

10 Summary

A measurement of the top quark–antiquark pair production cross section $\sigma_{\mathrm{t\bar{t}}}$ by the CMS Collaboration in proton–proton collisions at a centre-of-mass energy of 13 TeV is presented, corresponding to an integrated luminosity of $35.9\,\mathrm{fb}^{-1}$. Assuming a top quark mass in the simulation of $m_{\mathrm{t}}^{\mathrm{MC}} = 172.5$ GeV, a visible cross section is measured in the fiducial region using dilepton events ($\mathrm{e}^{\pm}\mu^{\mp}$, $\mu^{+}\mu^{-}$, $\mathrm{e}^{+}\mathrm{e}^{-}$) and then extrapolated to the full phase space. The total $\mathrm{t\bar{t}}$ production cross section is found to be $\sigma_{\mathrm{t\bar{t}}} = 803 \pm 2\,(\mathrm{stat}) \pm 25\,(\mathrm{syst}) \pm 20\,(\mathrm{lumi})$ pb. The measurement is in good agreement with the theoretical prediction calculated to next-to-next-to-leading order in perturbative QCD, including soft-gluon resummation to next-to-next-to-leading logarithm.

The measurement is repeated including the top quark mass in the POWHEG simulation as an additional free parameter in the fit. The sensitivity to $m_{\mathrm{t}}^{\mathrm{MC}}$ is maximized by fitting the minimum invariant mass found when combining the charged leptons with the b jets in an event. This yields a cross section of $\sigma_{\mathrm{t\bar{t}}} = 815 \pm 2\,(\mathrm{stat}) \pm 29\,(\mathrm{syst}) \pm 20\,(\mathrm{lumi})$ pb and a value of $m_{\mathrm{t}}^{\mathrm{MC}} = 172.33 \pm 0.14\,(\mathrm{stat})\,^{+0.66}_{-0.72}\,(\mathrm{syst})$ GeV, in good agreement with previous measurements. The value of $\sigma_{\mathrm{t\bar{t}}}$ obtained in the simultaneous fit is further used to extract the values of the top quark mass and the strong coupling constant at next-to-next-to-leading order in the minimal subtraction renormalization scheme, as well as the value of the

top quark pole mass for different sets of parton distribution functions.

Acknowledgements We congratulate our colleagues in the CERN accelerator departments for the excellent performance of the LHC and thank the technical and administrative staffs at CERN and at other CMS institutes for their contributions to the success of the CMS effort. In addition, we gratefully acknowledge the computing centres and personnel of the Worldwide LHC Computing Grid for delivering so effectively the computing infrastructure essential to our analyses. Finally, we acknowledge the enduring support for the construction and operation of the LHC and the CMS detector provided by the following funding agencies: BMBWF and FWF (Austria); FNRS and FWO (Belgium); CNPq, CAPES, FAPERJ, FAPERGS, and FAPESP (Brazil); MES (Bulgaria); CERN; CAS, MoST, and NSFC (China); COLCIENCIAS (Colombia); MSES and CSF (Croatia); RPF (Cyprus); SENESCYT (Ecuador); MoER, ERC IUT, and ERDF (Estonia); Academy of Finland, MEC, and HIP (Finland); CEA and CNRS/IN2P3 (France); BMBF, DFG, and HGF (Germany); GSRT (Greece); NKFIA (Hungary); DAE and DST (India); IPM (Iran); SFI (Ireland); INFN (Italy); MSIP and NRF (Republic of Korea); MES (Latvia); LAS (Lithuania); MOE and UM (Malaysia); BUAP, CINVESTAV, CONACYT, LNS, SEP, and UASLP-FAI (Mexico); MOS (Montenegro); MBIE (New Zealand); PAEC (Pakistan); MSHE and NSC (Poland); FCT (Portugal); JINR (Dubna); MON, RosAtom, RAS, RFBR, and NRC KI (Russia); MESTD (Serbia); SEIDI, CPAN, PCTI, and FEDER (Spain); MOSTR (Sri Lanka); Swiss Funding Agencies (Switzerland); MST (Taipei); ThEPCenter, IPST, STAR, and NSTDA (Thailand); TUBITAK and TAEK (Turkey); NASU and SFFR (Ukraine); STFC (United Kingdom); DOE and NSF (USA). Individuals have received support from the Marie-Curie programme and the European Research Council and Horizon 2020 Grant, contract No. 675440 (European Union); the Leventis Foundation; the A.P. Sloan Foundation; the Alexander von Humboldt Foundation; the Belgian Federal Science Policy Office; the Fonds pour la Formation à la Recherche dans l'Industrie et dans l'Agriculture (FRIA-Belgium); the Agentschap voor Innovatie door Wetenschap en Technologie (IWT-Belgium); the F.R.S.-FNRS and FWO (Belgium) under the "Excellence of Science – EOS" – be.h project n. 30820817; the Ministry of Education, Youth and Sports (MEYS) of the Czech Republic; the Lendület ("Momentum") Programme and the János Bolyai Research Scholarship of the Hungarian Academy of Sciences, the New National Excellence Program ÚNKP, the NKFIA research grants 123842, 123959, 124845, 124850, and 125105 (Hungary); the Council of Science and Industrial Research, India; the HOMING PLUS programme of the Foundation for Polish Science, cofinanced from European Union, Regional Development Fund, the Mobility Plus programme of the Ministry of Science and Higher Education, the National Science Center (Poland), contracts Harmonia 2014/14/M/ST2/00428, Opus 2014/13/B/ST2/02543, 2014/15/B/ST2/03998, and 2015/19/B/ST2/02861, Sonata-bis 2012/07/E/ST2/01406; the National Priorities Research Program by Qatar National Research Fund; the Programa Estatal de Fomento de la Investigación Científica y Técnica de Excelencia María de Maeztu, grant MDM-2015-0509 and the Programa Severo Ochoa del Principado de Asturias; the Thalis and Aristeia programmes cofinanced by EU-ESF and the Greek NSRF; the Rachadapisek Sompot Fund for Postdoctoral Fellowship, Chulalongkorn University and the Chulalongkorn Academic into Its 2nd Century Project Advancement Project (Thailand); the Welch Foundation, contract C-1845; and the Weston Havens Foundation (USA).

Data Availability Statement This manuscript has no associated data or the data will not be deposited . [Authors' comment: Release and preservation of data used by the CMS Collaboration as the basis for publications is guided by the CMS policy as written in its document "CMS data preservation, re-use and open access policy" (https://cms-docdb.cern.ch/cgi-bin/PublicDocDB/RetrieveFile?docid=6032&filename=CMSDataPolicyV1.2.pdf&version=2).]

Funded by SCOAP[3].

References

1. ATLAS Collaboration, Measurement of the $t\bar{t}$ production cross-section using $e\mu$ events with b-tagged jets in pp collisions at $\sqrt{s} = 7$ and 8 TeV with the ATLAS detector. Eur. Phys. J. C **74** 3109 (2014). https://doi.org/10.1140/epjc/s10052-014-3109-7. arXiv:1406.5375. [Addendum: https://doi.org/10.1140/epjc/s10052-016-4501-2]
2. ATLAS Collaboration, Measurement of the $t\bar{t}$ production cross-section using $e\mu$ events with b-tagged jets in pp collisions at $\sqrt{s} = 13$ TeV with the ATLAS detector. Phys. Lett. B **761** 136 (2016). https://doi.org/10.1016/j.physletb.2016.08.019, arXiv:1606.02699. [Erratum: https://doi.org/10.1016/j.physletb.2017.09.027]
3. CMS Collaboration, Measurement of the inclusive $t\bar{t}$ cross section in pp collisions at $\sqrt{s} = 5.02$ TeV using final states with at least one charged lepton. JHEP **03** 115 (2018). https://doi.org/10.1007/JHEP03(2018)115. arXiv:1711.03143
4. CMS Collaboration, Measurement of the $t\bar{t}$ production cross section in the $e\mu$ channel in proton–proton collisions at $\sqrt{s} = 7$ and 8 TeV. JHEP **08**, 029 (2016). https://doi.org/10.1007/JHEP08(2016)029. arXiv:1603.02303
5. CMS Collaboration, Measurement of the $t\bar{t}$ production cross section using events with one lepton and at least one jet in pp collisions at $\sqrt{s} = 13$ TeV. JHEP **09**, 051 (2017). https://doi.org/10.1007/JHEP09(2017)051. arXiv:1701.06228
6. P. Bärnreuther, M. Czakon, A. Mitov, Percent-level-precision physics at the Tevatron: next-to-next-to-leading order QCD corrections to $q\bar{q} \to t\bar{t} + X$. Phys. Rev. Lett. **109**, 132001 (2012). https://doi.org/10.1103/PhysRevLett.109.132001. arXiv:1204.5201
7. M. Czakon, A. Mitov, NNLO corrections to top-pair production at hadron colliders: the all-fermionic scattering channels. JHEP **12**, 054 (2012). https://doi.org/10.1007/JHEP12(2012)054. arXiv:1207.0236
8. M. Czakon, A. Mitov, NNLO corrections to top pair production at hadron colliders: the quark–gluon reaction. JHEP **01**, 080 (2013). https://doi.org/10.1007/JHEP01(2013)080. arXiv:1210.6832
9. M. Czakon, P. Fiedler, A. Mitov, Total top-quark pair-production cross section at hadron colliders through $O(\alpha_S^4)$. Phys. Rev. Lett. **110**, 252004 (2013). https://doi.org/10.1103/PhysRevLett.110.252004. arXiv:1303.6254
10. D0 Collaboration, Determination of the pole and $\bar{M}S$ masses of the top quark from the $t\bar{t}$ cross section. Phys. Lett. B **703**, 422 (2011). https://doi.org/10.1016/j.physletb.2011.08.015. arXiv:1104.2887
11. CMS Collaboration, Determination of the top-quark pole mass and strong coupling constant from the $t\bar{t}$ production cross section in pp collisions at $\sqrt{s} = 7$ TeV. Phys. Lett. B **728**, 496 (2014). https://doi.org/10.1016/j.physletb.2013.12.009. arXiv:1307.1907. [Erratum: https://doi.org/10.1016/j.physletb.2014.08.040]
12. D0 Collaboration, Measurement of the inclusive $t\bar{t}$ production cross section in $p\bar{p}$ collisions at $\sqrt{s} = 1.96$ TeV and determination of the top quark pole mass. Phys. Rev. D **94** (2016) 092004. https://doi.org/10.1103/PhysRevD.94.092004. arXiv:1605.06168
13. T. Klijnsma, S. Bethke, G. Dissertori, G.P. Salam, Determination of the strong coupling constant $\alpha_S(m_Z)$ from measurements of the

total cross section for top-antitop quark production. Eur. Phys. J. C **77**, 778 (2017). https://doi.org/10.1140/epjc/s10052-017-5340-5. arXiv:1708.07495
14. M. Czakon, M.L. Mangano, A. Mitov, J. Rojo, Constraints on the gluon PDF from top quark pair production at hadron colliders. JHEP **07**, 167 (2013). https://doi.org/10.1007/JHEP07(2013)167. arXiv:1303.7215
15. M. Guzzi, K. Lipka, S.-O. Moch, Top-quark pair production at hadron colliders: differential cross section and phenomenological applications with DiffTop. JHEP **01**, 082 (2015). https://doi.org/10.1007/JHEP01(2015)082. arXiv:1406.0386
16. CMS Collaboration, Measurement of double-differential cross sections for top quark pair production in pp collisions at $\sqrt{s} = 8TeV$ and impact on parton distribution functions. Eur. Phys. J. C **77**, 459 (2017). https://doi.org/10.1140/epjc/s10052-017-4984-5. arXiv:1703.01630
17. S. Alekhin, J. Blumlein, S. Moch, R. Placakyte, Parton distribution functions, a_S, and heavy-quark masses for LHC Run II. Phys. Rev. D **96**, 014011 (2017). https://doi.org/10.1103/PhysRevD.96.014011. arXiv:1701.05838
18. Gfitter Group Collaboration, The global electroweak fit at NNLO and prospects for the LHC and ILC. Eur. Phys. J. C **74**, 3046 (2014). https://doi.org/10.1140/epjc/s10052-014-3046-5. arXiv:1407.3792
19. G. Degrassi et al., Higgs mass and vacuum stability in the standard model at NNLO. JHEP **08**, 098 (2012). https://doi.org/10.1007/JHEP08(2012)098. arXiv:1205.6497
20. M. Dowling, S.-O. Moch, Differential distributions for top-quark hadro-production with a running mass. Eur. Phys. J. C **74**, 3167 (2014). https://doi.org/10.1140/epjc/s10052-014-3167-x. arXiv:1305.6422
21. P. Marquard, A.V. Smirnov, V.A. Smirnov, M. Steinhauser, Quark mass relations to four-loop order in perturbative QCD. Phys. Rev. Lett. **114**, 142002 (2015). https://doi.org/10.1103/PhysRevLett.114.142002. arXiv:1502.01030
22. CDF and D0 Collaborations, Combination of CDF and D0 results on the mass of the top quark using up 9.7fb^{-1} at the Tevatron (2016). arXiv:1608.01881
23. ATLAS Collaboration, Measurement of the top quark mass in the $t\bar{t} \to$ dilepton channel from $\sqrt{s} = 8$ TeV ATLAS data. Phys. Lett. B **761** (2016) 350, https://doi.org/10.1016/j.physletb.2016.08.042. arXiv:1606.02179
24. ATLAS, CDF, CMS and D0 Collaborations, First combination of Tevatron and LHC measurements of the top-quark mass (2014). arXiv:1403.4427
25. CMS Collaboration, Measurement of the top quark mass using proton–proton data at $\sqrt{s} = 7$ and 8 TeV. Phys. Rev. D **93**, 072004 (2016). https://doi.org/10.1103/PhysRevD.93.072004. arXiv:1509.04044
26. CMS Collaboration, Measurement of masses in the $t\bar{t}$ system by kinematic endpoints in pp collisions at $\sqrt{s} = 7TeV$. Eur. Phys. J. C **73**, 2494 (2013). https://doi.org/10.1140/epjc/s10052-013-2494-7. arXiv:1304.5783
27. A. Buckley et al., General-purpose event generators for LHC physics. Phys. Rep. **504**, 145 (2011). https://doi.org/10.1016/j.physrep.2011.03.005. arXiv:1101.2599
28. A.H. Hoang, S. Plätzer, D. Samitz, On the cutoff dependence of the quark mass parameter in angular ordered parton showers. JHEP **10**, 200 (2018). https://doi.org/10.1007/JHEP10(2018)200. arXiv:1807.06617
29. Particle Data Group, M. Tanabashi et al., Review of particle physics. Phys. Rev. D **98** 030001 (2018).https://doi.org/10.1103/PhysRevD.98.030001
30. J. Kieseler, K. Lipka, S.-O. Moch, Calibration of the top-quark Monte Carlo mass. Phys. Rev. Lett. **116**, 162001 (2016). https://doi.org/10.1103/PhysRevLett.116.162001. arXiv:1511.00841
31. CMS Collaboration, Measurement of the top quark mass with lepton+jets final states using pp collisions at $\sqrt{s} = 13TeV$. Eur. Phys. J. C **78**, 891 (2018). https://doi.org/10.1140/epjc/s10052-018-6332-9. arXiv:1805.01428
32. CMS Collaboration, The CMS experiment at the CERN LHC. JINST **3**, S08004 (2008). https://doi.org/10.1088/1748-0221/3/08/S08004
33. CMS Collaboration, The CMS trigger system. JINST **12**, P01020 (2017). https://doi.org/10.1088/1748-0221/12/01/P01020. arXiv:1609.02366
34. S. Alioli, P. Nason, C. Oleari, E. Re, A general framework for implementing NLO calculations in shower Monte Carlo programs: the POWHEG BOX. JHEP **06**, 043 (2010). https://doi.org/10.1007/JHEP06(2010)043. arXiv:1002.2581
35. S. Frixione, P. Nason, C. Oleari, Matching NLO QCD computations with parton shower simulations: the powheg method. JHEP **11**, 070 (2007). https://doi.org/10.1088/1126-6708/2007/11/070. arXiv:0709.2092
36. P. Nason, A new method for combining NLO QCD with shower Monte Carlo algorithms. JHEP **11**, 040 (2004). https://doi.org/10.1088/1126-6708/2004/11/040. arXiv:hep-ph/0409146
37. S. Frixione, P. Nason, G. Ridolfi, A positive-weight next-to-leading-order Monte Carlo for heavy flavour hadroproduction. JHEP **09**, 126 (2007). https://doi.org/10.1088/1126-6708/2007/09/126. arXiv:0707.3088
38. NNPDF Collaboration, Parton distributions with LHC data. Nucl. Phys. B **867**, 244 (2013). https://doi.org/10.1016/j.nuclphysb.2012.10.003. arXiv:1207.1303
39. T. Sjöstrand et al., An introduction to PYTHIA 8.2. Comput. Phys. Commun. **191**, 159 (2015). https://doi.org/10.1016/j.cpc.2015.01.024. arXiv:1410.3012
40. CMS Collaboration, Investigations of the impact of the parton shower tuning in PYTHIA 8 in the modelling of $t\bar{t}$ at $\sqrt{s} = 8$ and 13 TeV. CMS Physics Analysis Summary CMS-PAS-TOP-16-021 (2016)
41. P. Skands, S. Carrazza, J. Rojo, Tuning pythia 8.1: the Monash, tune. Eur. Phys. J. C **74**(2014), 3024 (2013). https://doi.org/10.1140/epjc/s10052-014-3024-y. arXiv:1404.5630
42. A. Kardos, P. Nason, C. Oleari, Three-jet production in powheg. JHEP **04**, 043 (2014). https://doi.org/10.1007/JHEP04(2014)043. arXiv:1402.4001
43. E. Re, Single-top Wt-channel production matched with parton showers using the powheg method. Eur. Phys. J. C **71**, 1547 (2011). https://doi.org/10.1140/epjc/s10052-011-1547-z. arXiv:1009.2450
44. S. Alioli, P. Nason, C. Oleari, E. Re, Vector boson plus one jet production in powheg. JHEP **01**, 095 (2011). https://doi.org/10.1007/JHEP01(2011)095. arXiv:1009.5594
45. CMS Collaboration, Event generator tunes obtained from underlying event and multiparton scattering measurements. Eur. Phys. J. C **76**, 155 (2016). https://doi.org/10.1140/epjc/s10052-016-3988-x. arXiv:1512.00815
46. J. Alwall et al., The automated computation of tree-level and next-to-leading order differential cross sections, and their matching to parton shower simulations. JHEP **07**, 079 (2014). https://doi.org/10.1007/JHEP07(2014)079. arXiv:1405.0301
47. S. Frixione, B.R. Webber, Matching NLO QCD computations and parton shower simulations. JHEP **06**, 029 (2002). https://doi.org/10.1088/1126-6708/2002/06/029. arXiv:hep-ph/0204244
48. ATLAS Collaboration, Measurement of the inelastic proton–proton cross section at $\sqrt{s} = 13$ TeV with the ATLAS detector at the LHC. Phys. Rev. Lett. **117** (2016) 182002. https://doi.org/10.1103/PhysRevLett.117.182002. arXiv:1606.02625
49. R. Gavin, Y. Li, F. Petriello, S. Quackenbush, FEWZ 2.0: a code for hadronic Z production at next-to-next-to-leading order. Comput.

Phys. Commun. **182**, 2388 (2011). https://doi.org/10.1016/j.cpc.2011.06.008. arXiv:1011.3540
50. N. Kidonakis, Two-loop soft anomalous dimensions for single top quark associated production with W^- or H^-. Phys. Rev. D **82**, 054018 (2010). https://doi.org/10.1103/PhysRevD.82.054018. arXiv:hep-ph/1005.4451
51. J.M. Campbell, R.K. Ellis, C. Williams, Vector boson pair production at the LHC. JHEP **07**, 018 (2011). https://doi.org/10.1007/JHEP07(2011)018. arXiv:1105.0020
52. M. Czakon, A. Mitov, Top++: a program for the calculation of the top-pair cross-section at hadron colliders. Comput. Phys. Commun. **185**, 2930 (2014). https://doi.org/10.1016/j.cpc.2014.06.021. arXiv:1112.5675
53. S. Dulat et al., New parton distribution functions from a global analysis of quantum chromodynamics. Phys. Rev. D **93**, 033006 (2016). https://doi.org/10.1103/PhysRevD.93.033006. arXiv:1506.07443
54. CMS Collaboration, Particle-flow reconstruction and global event description with the CMS detector. JINST **12**, P10003 (2017). https://doi.org/10.1088/1748-0221/12/10/P10003. arXiv:1706.04965
55. CMS Collaboration, Performance of electron reconstruction and selection with the CMS detector in proton–proton collisions at $\sqrt{s} = 8$ TeV. JINST **10**, P06005 (2015). https://doi.org/10.1088/1748-0221/10/06/P06005. arXiv:1502.02701
56. CMS Collaboration, Performance of the CMS muon detector and muon reconstruction with proton–proton collisions at $\sqrt{s} = 13$ TeV. JINST **13**, P06015 (2018). https://doi.org/10.1088/1748-0221/13/06/P06015. arXiv:1804.04528
57. M. Cacciari, G.P. Salam, G. Soyez, The anti-k_T jet clustering algorithm. JHEP **04**, 063 (2008). https://doi.org/10.1088/1126-6708/2008/04/063. arXiv:0802.1189
58. M. Cacciari, G.P. Salam, G. Soyez, FastJet user manual. Eur. Phys. J. C **72**, 1896 (2012). https://doi.org/10.1140/epjc/s10052-012-1896-2. arXiv:1111.6097
59. CMS Collaboration, Jet energy scale and resolution in the CMS experiment in pp collisions at 8 TeV. JINST **12**, P02014 (2017). https://doi.org/10.1088/1748-0221/12/02/P02014. arXiv:1607.03663
60. CMS Collaboration, Identification of heavy-flavour jets with the CMS detector in pp collisions at 13 TeV. JINST **13**, P05011 (2018). https://doi.org/10.1088/1748-0221/13/05/P05011. arXiv:1712.07158
61. F. James, M. Roos, Minuit: a system for function minimization and analysis of the parameter errors and correlations. Comput. Phys. Commun. **10**, 343 (1975). https://doi.org/10.1016/0010-4655(75)90039-9
62. CMS Collaboration, Jet algorithms performance in 13 TeV data. CMS physics analysis summary CMS-PAS-JME-16-003 (2017). http://cds.cern.ch/record/2256875
63. CMS Collaboration, CMS luminosity measurements for the 2016 data taking period. CMS physics analysis summary CMS-PAS-LUM-17-001 (2017). http://cds.cern.ch/record/2257069
64. M. Cacciari et al., The $\mathrm{t\bar{t}}$ cross-section at 1.8 TeV and 1.96 TeV: a study of the systematics due to parton densities and scale dependence. JHEP **04**, 068 (2004). https://doi.org/10.1088/1126-6708/2004/04/068. arXiv:hep-ph/0303085
65. S. Catani, D. de Florian, M. Grazzini, P. Nason, Soft gluon resummation for Higgs boson production at hadron colliders. JHEP **07**, 028 (2003). https://doi.org/10.1088/1126-6708/2003/07/028. arXiv:hep-ph/0306211
66. R. Frederix, S. Frixione, Merging meets matching in mc@nlo. JHEP **12**, 061 (2012). https://doi.org/10.1007/JHEP12(2012)061. arXiv:1209.6215
67. CMS Collaboration, Measurements of $\mathrm{t\bar{t}}$ differential cross sections in proton–proton collisions at $\sqrt{s} = 13$ TeV using events containing two leptons. JHEP **02**, 149 (2019). https://doi.org/10.1007/JHEP02(2019)149. arXiv:1811.06625
68. CMS Collaboration, Measurement of normalized differential $\mathrm{t\bar{t}}$ cross sections in the dilepton channel from pp collisions at $\sqrt{s} = 13$ TeV. JHEP **04**, 060 (2018). https://doi.org/10.1007/JHEP04(2018)060. arXiv:1708.07638
69. CMS Collaboration, Measurement of differential cross sections for top quark pair production using the lepton+jets final state in proton–proton collisions at 13 TeV. Phys. Rev. D **95**, 092001 (2017). https://doi.org/10.1103/PhysRevD.95.092001. arXiv:1610.04191
70. M.G. Bowler, e^+e^- production of heavy quarks in the string model. Z. Phys. C **11**, 169 (1981). https://doi.org/10.1007/BF01574001
71. C. Peterson, D. Schlatter, I. Schmitt, P.M. Zerwas, Scaling violations in inclusive e^+e^- annihilation spectra. Phys. Rev. D **27**, 105 (1983). https://doi.org/10.1103/PhysRevD.27.105
72. S. Argyropoulos, T. Sjöstrand, Effects of color reconnection on $\mathrm{t\bar{t}}$ final states at the LHC. JHEP **11**, 043 (2014). https://doi.org/10.1007/JHEP11(2014)043. arXiv:1407.6653
73. J.R. Christiansen, P.Z. Skands, String formation beyond leading colour. JHEP **08**, 003 (2015). https://doi.org/10.1007/JHEP08(2015)003. arXiv:1505.01681
74. CMS Collaboration, Measurement of the top quark pair production cross section in proton–proton collisions at $\sqrt{s} = 13$ TeV. Phys. Rev. Lett. **116**, 052002 (2016). https://doi.org/10.1103/PhysRevLett.116.052002. arXiv:1510.05302
75. CMS Collaboration, Measurement of the $\mathrm{t\bar{t}}$ production cross section using events in the $e\mu$ final state in pp collisions at $\sqrt{s} = 13$ TeV. Eur. Phys. J. C **77**, 172 (2017). https://doi.org/10.1140/epjc/s10052-017-4718-8. arXiv:1611.04040
76. S. Alekhin et al., HERAFitter. Eur. Phys. J. C **75**, 304 (2015). https://doi.org/10.1140/epjc/s10052-015-3480-z. arXiv:1410.4412
77. H1 and ZEUS Collaborations, Combination of measurements of inclusive deep inelastic $e^{\pm}p$ scattering cross sections and QCD analysis of HERA data. Eur. Phys. J. C **75**, 580 (2015). https://doi.org/10.1140/epjc/s10052-015-3710-4. arXiv:1506.06042
78. CMS Collaboration, Measurement and QCD analysis of double-differential inclusive jet cross sections in pp collisions at $\sqrt{s} = 8$ TeV and cross section ratios to 2.76 and 7 TeV. JHEP **03** 156 (2017). https://doi.org/10.1007/JHEP03(2017)156. arXiv:1609.05331
79. M. Aliev et al., Hathor: HAdronic top and heavy quarks crOss section calculatoR. Comput. Phys. Commun. **182**, 1034 (2011). https://doi.org/10.1016/j.cpc.2010.12.040. arXiv:1007.1327
80. A. Buckley et al., LHAPDF6: parton density access in the LHC precision era. Eur. Phys. J. C **75**, 132 (2015). https://doi.org/10.1140/epjc/s10052-015-3318-8. arXiv:1412.7420
81. L.A. Harland-Lang, A.D. Martin, P. Motylinski, R.S. Thorne, Parton distributions in the LHC era: MMHT 2014 PDFs. Eur. Phys. J. C **75**, 204 (2015). https://doi.org/10.1140/epjc/s10052-015-3397-6. arXiv:1412.3989
82. NNPDF Collaboration, Parton distributions from high-precision collider data. Eur. Phys. J. C **77**, 663 (2017). https://doi.org/10.1140/epjc/s10052-017-5199-5. arXiv:1706.00428
83. K.G. Chetyrkin, J.H. Kuhn, M. Steinhauser, RunDec: a Mathematica package for running and decoupling of the strong coupling and quark masses. Comput. Phys. Commun. **133**, 43 (2000). https://doi.org/10.1016/S0010-4655(00)00155-7. arXiv:hep-ph/0004189
84. B. Schmidt, M. Steinhauser, C RunDec: a C++ package for running and decoupling of the strong coupling and quark masses. Comput. Phys. Commun. **183**, 1845 (2012). https://doi.org/10.1016/j.cpc.2012.03.023. arXiv:1201.6149
85. H1 Collaboration, Determination of the strong coupling constant $a_S(m_Z)$ in next-to-next-to-leading order QCD using H1 jet cross section measurements. Eur. Phys. J. C **77**, 791 (2017). https://doi.org/10.1140/epjc/s10052-017-5314-7. arXiv:1709.07251

CMS Collaboration

Yerevan Physics Institute, Yerevan, Armenia
A. M. Sirunyan, A. Tumasyan

Institut für Hochenergiephysik, Wien, Austria
W. Adam, F. Ambrogi, E. Asilar, T. Bergauer, J. Brandstetter, M. Dragicevic, J. Erö, A. Escalante Del Valle, M. Flechl, R. Frühwirth[1], V. M. Ghete, J. Hrubec, M. Jeitler[1], N. Krammer, I. Krätschmer, D. Liko, T. Madlener, I. Mikulec, N. Rad, H. Rohringer, J. Schieck[1], R. Schöfbeck, M. Spanring, D. Spitzbart, W. Waltenberger, J. Wittmann, C.-E. Wulz[1], M. Zarucki

Institute for Nuclear Problems, Minsk, Belarus
V. Chekhovsky, V. Mossolov, J. Suarez Gonzalez

Universiteit Antwerpen, Antwerpen, Belgium
E. A. De Wolf, D. Di Croce, X. Janssen, J. Lauwers, A. Lelek, M. Pieters, H. Van Haevermaet, P. Van Mechelen, N. Van Remortel

Vrije Universiteit Brussel, Brussels, Belgium
S. Abu Zeid, F. Blekman, J. D'Hondt, J. De Clercq, K. Deroover, G. Flouris, D. Lontkovskyi, S. Lowette, I. Marchesini, S. Moortgat, L. Moreels, Q. Python, K. Skovpen, S. Tavernier, W. Van Doninck, P. Van Mulders, I. Van Parijs

Université Libre de Bruxelles, Brussels, Belgium
D. Beghin, B. Bilin, H. Brun, B. Clerbaux, G. De Lentdecker, H. Delannoy, B. Dorney, G. Fasanella, L. Favart, A. Grebenyuk, A. K. Kalsi, T. Lenzi, J. Luetic, N. Postiau, E. Starling, L. Thomas, C. Vander Velde, P. Vanlaer, D. Vannerom, Q. Wang

Ghent University, Ghent, Belgium
T. Cornelis, D. Dobur, A. Fagot, M. Gul, I. Khvastunov[2], D. Poyraz, C. Roskas, D. Trocino, M. Tytgat, W. Verbeke, B. Vermassen, M. Vit, N. Zaganidis

Université Catholique de Louvain, Louvain-la-Neuve, Belgium
H. Bakhshiansohi, O. Bondu, G. Bruno, C. Caputo, P. David, C. Delaere, M. Delcourt, A. Giammanco, G. Krintiras, V. Lemaitre, A. Magitteri, K. Piotrzkowski, A. Saggio, M. Vidal Marono, P. Vischia, J. Zobec

Centro Brasileiro de Pesquisas Fisicas, Rio de Janeiro, Brazil
F. L. Alves, G. A. Alves, G. Correia Silva, C. Hensel, A. Moraes, M. E. Pol, P. Rebello Teles

Universidade do Estado do Rio de Janeiro, Rio de Janeiro, Brazil
E. Belchior Batista Das Chagas, W. Carvalho, J. Chinellato[3], E. Coelho, E. M. Da Costa, G. G. Da Silveira[4], D. De Jesus Damiao, C. De Oliveira Martins, S. Fonseca De Souza, H. Malbouisson, D. Matos Figueiredo, M. Melo De Almeida, C. Mora Herrera, L. Mundim, H. Nogima, W. L. Prado Da Silva, L. J. Sanchez Rosas, A. Santoro, A. Sznajder, M. Thiel, E. J. Tonelli Manganote[3], F. Torres Da Silva De Araujo, A. Vilela Pereira

Universidade Estadual Paulista [a], Universidade Federal do ABC [b], São Paulo, Brazil
S. Ahuja[a], C. A. Bernardes[a], L. Calligaris[a], T. R. Fernandez Perez Tomei[a], E. M. Gregores[b], P. G. Mercadante[b], S. F. Novaes[a], Sandra S. Padula[a]

Institute for Nuclear Research and Nuclear Energy, Bulgarian Academy of Sciences, Sofia, Bulgaria
A. Aleksandrov, R. Hadjiiska, P. Iaydjiev, A. Marinov, M. Misheva, M. Rodozov, M. Shopova, G. Sultanov

University of Sofia, Sofia, Bulgaria
A. Dimitrov, L. Litov, B. Pavlov, P. Petkov

Beihang University, Beijing, China
W. Fang[5], X. Gao[5], L. Yuan

Institute of High Energy Physics, Beijing, China
M. Ahmad, J. G. Bian, G. M. Chen, H. S. Chen, M. Chen, Y. Chen, C. H. Jiang, D. Leggat, H. Liao, Z. Liu, S. M. Shaheen[6], A. Spiezia, J. Tao, E. Yazgan, H. Zhang, S. Zhang[6], J. Zhao

State Key Laboratory of Nuclear Physics and Technology, Peking University, Beijing, China
Y. Ban, G. Chen, A. Levin, J. Li, L. Li, Q. Li, Y. Mao, S. J. Qian, D. Wang

Tsinghua University, Beijing, China
Y. Wang

Universidad de Los Andes, Bogotá, Colombia
C. Avila, A. Cabrera, C. A. Carrillo Montoya, L. F. Chaparro Sierra, C. Florez, C. F. González Hernández, M. A. Segura Delgado

Faculty of Electrical Engineering, Mechanical Engineering and Naval Architecture, University of Split, Split, Croatia
B. Courbon, N. Godinovic, D. Lelas, I. Puljak, T. Sculac

Faculty of Science, University of Split, Split, Croatia
Z. Antunovic, M. Kovac

Institute Rudjer Boskovic, Zagreb, Croatia
V. Brigljevic, D. Ferencek, K. Kadija, B. Mesic, M. Roguljic, A. Starodumov[7], T. Susa

University of Cyprus, Nicosia, Cyprus
M. W. Ather, A. Attikis, M. Kolosova, G. Mavromanolakis, J. Mousa, C. Nicolaou, F. Ptochos, P. A. Razis, H. Rykaczewski

Charles University, Prague, Czech Republic
M. Finger[8], M. Finger Jr.[8]

Escuela Politecnica Nacional, Quito, Ecuador
E. Ayala

Universidad San Francisco de Quito, Quito, Ecuador
E. Carrera Jarrin

Academy of Scientific Research and Technology of the Arab Republic of Egypt, Egyptian Network of High Energy Physics, Cairo, Egypt
H. Abdalla[9], A. Mohamed[10], E. Salama[11,12]

National Institute of Chemical Physics and Biophysics, Tallinn, Estonia
S. Bhowmik, A. Carvalho Antunes De Oliveira, R. K. Dewanjee, K. Ehataht, M. Kadastik, M. Raidal, C. Veelken

Department of Physics, University of Helsinki, Helsinki, Finland
P. Eerola, H. Kirschenmann, J. Pekkanen, M. Voutilainen

Helsinki Institute of Physics, Helsinki, Finland
J. Havukainen, J. K. Heikkilä, T. Järvinen, V. Karimäki, R. Kinnunen, T. Lampén, K. Lassila-Perini, S. Laurila, S. Lehti, T. Lindén, P. Luukka, T. Mäenpää, H. Siikonen, E. Tuominen, J. Tuominiemi

Lappeenranta University of Technology, Lappeenranta, Finland
T. Tuuva

IRFU, CEA, Université Paris-Saclay, Gif-sur-Yvette, France
M. Besancon, F. Couderc, M. Dejardin, D. Denegri, J. L. Faure, F. Ferri, S. Ganjour, A. Givernaud, P. Gras, G. Hamel de Monchenault, P. Jarry, C. Leloup, E. Locci, J. Malcles, G. Negro, J. Rander, A. Rosowsky, M. Ö. Sahin, M. Titov

Laboratoire Leprince-Ringuet, Ecole polytechnique, CNRS/IN2P3, Université Paris-Saclay, Palaiseau, France
A. Abdulsalam[13], C. Amendola, I. Antropov, F. Beaudette, P. Busson, C. Charlot, R. Granier de Cassagnac, I. Kucher, A. Lobanov, J. Martin Blanco, C. Martin Perez, M. Nguyen, C. Ochando, G. Ortona, P. Paganini, J. Rembser, R. Salerno, J. B. Sauvan, Y. Sirois, A. G. Stahl Leiton, A. Zabi, A. Zghiche

Université de Strasbourg, CNRS, IPHC UMR 7178, Strasbourg, France
J.-L. Agram[14], J. Andrea, D. Bloch, G. Bourgatte, J.-M. Brom, E. C. Chabert, V. Cherepanov, C. Collard, E. Conte[14], J.-C. Fontaine[14], D. Gelé, U. Goerlach, M. Jansová, A.-C. Le Bihan, N. Tonon, P. Van Hove

Centre de Calcul de l'Institut National de Physique Nucleaire et de Physique des Particules, CNRS/IN2P3, Villeurbanne, France
S. Gadrat

Université de Lyon, Université Claude Bernard Lyon 1, CNRS-IN2P3, Institut de Physique Nucléaire de Lyon, Villeurbanne, France
S. Beauceron, C. Bernet, G. Boudoul, N. Chanon, R. Chierici, D. Contardo, P. Depasse, H. El Mamouni, J. Fay, L. Finco, S. Gascon, M. Gouzevitch, G. Grenier, B. Ille, F. Lagarde, I. B. Laktineh, H. Lattaud, M. Lethuillier, L. Mirabito, S. Perries, A. Popov[15], V. Sordini, G. Touquet, M. Vander Donckt, S. Viret

Georgian Technical University, Tbilisi, Georgia
A. Khvedelidze[8]

Tbilisi State University, Tbilisi, Georgia
Z. Tsamalaidze[8]

RWTH Aachen University, I. Physikalisches Institut, Aachen, Germany
C. Autermann, L. Feld, M. K. Kiesel, K. Klein, M. Lipinski, M. Preuten, M. P. Rauch, C. Schomakers, J. Schulz, M. Teroerde, B. Wittmer

RWTH Aachen University, III. Physikalisches Institut A, Aachen, Germany
A. Albert, M. Erdmann, S. Erdweg, T. Esch, R. Fischer, S. Ghosh, T. Hebbeker, C. Heidemann, K. Hoepfner, H. Keller, L. Mastrolorenzo, M. Merschmeyer, A. Meyer, P. Millet, S. Mukherjee, T. Pook, A. Pozdnyakov, M. Radziej, H. Reithler, M. Rieger, A. Schmidt, D. Teyssier, S. Thüer

RWTH Aachen University, III. Physikalisches Institut B, Aachen, Germany
G. Flügge, O. Hlushchenko, T. Kress, T. Müller, A. Nehrkorn, A. Nowack, C. Pistone, O. Pooth, D. Roy, H. Sert, A. Stahl[16]

Deutsches Elektronen-Synchrotron, Hamburg, Germany
M. Aldaya Martin, T. Arndt, C. Asawatangtrakuldee, I. Babounikau, K. Beernaert, O. Behnke, U. Behrens, A. Bermúdez Martínez, D. Bertsche, A. A. Bin Anuar, K. Borras[17], V. Botta, A. Campbell, P. Connor, C. Contreras-Campana, V. Danilov, A. De Wit, M. M. Defranchis, C. Diez Pardos, D. Domínguez Damiani, G. Eckerlin, T. Eichhorn, A. Elwood, E. Eren, E. Gallo[18], A. Geiser, J. M. Grados Luyando, A. Grohsjean, M. Guthoff, M. Haranko, A. Harb, H. Jung, M. Kasemann, J. Keaveney, C. Kleinwort, J. Knolle, D. Krücker, W. Lange, T. Lenz, J. Leonard, K. Lipka, W. Lohmann[19], R. Mankel, I.-A. Melzer-Pellmann, A. B. Meyer, M. Meyer, M. Missiroli, G. Mittag, J. Mnich, V. Myronenko, S. K. Pflitsch, D. Pitzl, A. Raspereza, A. Saibel, M. Savitskyi, P. Saxena, P. Schütze, C. Schwanenberger, R. Shevchenko, A. Singh, H. Tholen, O. Turkot, A. Vagnerini, M. Van De Klundert, G. P. Van Onsem, R. Walsh, Y. Wen, K. Wichmann, C. Wissing, O. Zenaiev

University of Hamburg, Hamburg, Germany
R. Aggleton, S. Bein, L. Benato, A. Benecke, T. Dreyer, A. Ebrahimi, E. Garutti, D. Gonzalez, P. Gunnellini, J. Haller, A. Hinzmann, A. Karavdina, G. Kasieczka, R. Klanner, R. Kogler, N. Kovalchuk, S. Kurz, V. Kutzner, J. Lange, D. Marconi, J. Multhaup, M. Niedziela, C.E.N. Niemeyer, D. Nowatschin, A. Perieanu, A. Reimers, O. Rieger, C. Scharf, P. Schleper, S. Schumann, J. Schwandt, J. Sonneveld, H. Stadie, G. Steinbrück, F. M. Stober, M. Stöver, B. Vormwald, I. Zoi

Karlsruher Institut fuer Technologie, Karlsruhe, Germany
M. Akbiyik, C. Barth, M. Baselga, S. Baur, E. Butz, R. Caspart, T. Chwalek, F. Colombo, W. De Boer, A. Dierlamm, K. El Morabit, N. Faltermann, B. Freund, M. Giffels, M. A. Harrendorf, F. Hartmann[16], S. M. Heindl, U. Husemann, I. Katkov[15], S. Kudella, S. Mitra, M. U. Mozer, Th. Müller, M. Musich, M. Plagge, G. Quast, K. Rabbertz, M. Schröder, I. Shvetsov, H. J. Simonis, R. Ulrich, S. Wayand, M. Weber, T. Weiler, C. Wöhrmann, R. Wolf

Institute of Nuclear and Particle Physics (INPP), NCSR Demokritos, Aghia Paraskevi, Greece
G. Anagnostou, G. Daskalakis, T. Geralis, A. Kyriakis, D. Loukas, G. Paspalaki

National and Kapodistrian University of Athens, Athens, Greece
A. Agapitos, G. Karathanasis, P. Kontaxakis, A. Panagiotou, I. Papavergou, N. Saoulidou, K. Vellidis

National Technical University of Athens, Athens, Greece
K. Kousouris, I. Papakrivopoulos, G. Tsipolitis

University of Ioánnina, Ioannina, Greece
I. Evangelou, C. Foudas, P. Gianneios, P. Katsoulis, P. Kokkas, S. Mallios, N. Manthos, I. Papadopoulos, E. Paradas, J. Strologas, F. A. Triantis, D. Tsitsonis

MTA-ELTE Lendület CMS Particle and Nuclear Physics Group, Eötvös Loránd University, Budapest, Hungary
M. Bartók[20], M. Csanad, N. Filipovic, P. Major, M. I. Nagy, G. Pasztor, O. Surányi, G. I. Veres

Wigner Research Centre for Physics, Budapest, Hungary
G. Bencze, C. Hajdu, D. Horvath[21], Á. Hunyadi, F. Sikler, T. Á. Vámi, V. Veszpremi, G. Vesztergombi[†]

Institute of Nuclear Research ATOMKI, Debrecen, Hungary
N. Beni, S. Czellar, J. Karancsi[20], A. Makovec, J. Molnar, Z. Szillasi

Institute of Physics, University of Debrecen, Debrecen, Hungary
P. Raics, Z. L. Trocsanyi, B. Ujvari

Indian Institute of Science (IISc), Bangalore, India
S. Choudhury, J. R. Komaragiri, P. C. Tiwari

National Institute of Science Education and Research, HBNI, Bhubaneswar, India
S. Bahinipati[23], C. Kar, P. Mal, K. Mandal, A. Nayak[24], S. Roy Chowdhury, D. K. Sahoo[23], S. K. Swain

Panjab University, Chandigarh, India
S. Bansal, S. B. Beri, V. Bhatnagar, S. Chauhan, R. Chawla, N. Dhingra, R. Gupta, A. Kaur, M. Kaur, S. Kaur, P. Kumari, M. Lohan, M. Meena, A. Mehta, K. Sandeep, S. Sharma, J. B. Singh, A. K. Virdi, G. Walia

University of Delhi, Delhi, India
A. Bhardwaj, B. C. Choudhary, R. B. Garg, M. Gola, S. Keshri, Ashok Kumar, S. Malhotra, M. Naimuddin, P. Priyanka, K. Ranjan, Aashaq Shah, R. Sharma

Saha Institute of Nuclear Physics, HBNI, Kolkata, India
R. Bhardwaj[25], M. Bharti[25], R. Bhattacharya, S. Bhattacharya, U. Bhawandeep[25], D. Bhowmik, S. Dey, S. Dutt[25], S. Dutta, S. Ghosh, M. Maity[26], K. Mondal, S. Nandan, A. Purohit, P. K. Rout, A. Roy, G. Saha, S. Sarkar, T. Sarkar[26], M. Sharan, B. Singh[25], S. Thakur[25]

Indian Institute of Technology Madras, Madras, India
P. K. Behera, A. Muhammad

Bhabha Atomic Research Centre, Mumbai, India
R. Chudasama, D. Dutta, V. Jha, V. Kumar, D. K. Mishra, P. K. Netrakanti, L. M. Pant, P. Shukla, P. Suggisetti

Tata Institute of Fundamental Research-A, Mumbai, India
T. Aziz, M. A. Bhat, S. Dugad, G. B. Mohanty, N. Sur, RavindraKumar Verma

Tata Institute of Fundamental Research-B, Mumbai, India
S. Banerjee, S. Bhattacharya, S. Chatterjee, P. Das, M. Guchait, Sa. Jain, S. Karmakar, S. Kumar, G. Majumder, K. Mazumdar, N. Sahoo

Indian Institute of Science Education and Research (IISER), Pune, India
S. Chauhan, S. Dube, V. Hegde, A. Kapoor, K. Kothekar, S. Pandey, A. Rane, A. Rastogi, S. Sharma

Institute for Research in Fundamental Sciences (IPM), Tehran, Iran
S. Chenarani[27], E. Eskandari Tadavani, S. M. Etesami[27], M. Khakzad, M. Mohammadi Najafabadi, M. Naseri, F. Rezaei Hosseinabadi, B. Safarzadeh[28], M. Zeinali

University College Dublin, Dublin, Ireland
M. Felcini, M. Grunewald

INFN Sezione di Bari[a], Università di Bari[b], Politecnico di Bari[c], Bari, Italy
M. Abbrescia[a,b], C. Calabria[a,b], A. Colaleo[a], D. Creanza[a,c], L. Cristella[a,b], N. De Filippis[a,c], M. De Palma[a,b], A. Di Florio[a,b], F. Errico[a,b], L. Fiore[a], A. Gelmi[a,b], G. Iaselli[a,c], M. Ince[a,b], S. Lezki[a,b], G. Maggi[a,c], M. Maggi[a], G. Miniello[a,b], S. My[a,b], S. Nuzzo[a,b], A. Pompili[a,b], G. Pugliese[a,c], R. Radogna[a], A. Ranieri[a], G. Selvaggi[a,b], A. Sharma[a], L. Silvestris[a], R. Venditti[a], P. Verwilligen[a]

INFN Sezione di Bologna[a], Università di Bologna[b], Bologna, Italy
G. Abbiendi[a], C. Battilana[a,b], D. Bonacorsi[a,b], L. Borgonovi[a,b], S. Braibant-Giacomelli[a,b], R. Campanini[a,b], P. Capiluppi[a,b], A. Castro[a,b], F. R. Cavallo[a], S. S. Chhibra[a,b], G. Codispoti[a,b], M. Cuffiani[a,b], G. M. Dallavalle[a], F. Fabbri[a], A. Fanfani[a,b], E. Fontanesi, P. Giacomelli[a], C. Grandi[a], L. Guiducci[a,b], F. Iemmi[a,b], S. Lo Meo[a,29], S. Marcellini[a], G. Masetti[a], A. Montanari[a], F. L. Navarria[a,b], A. Perrotta[a], F. Primavera[a,b], A. M. Rossi[a,b], T. Rovelli[a,b], G. P. Siroli[a,b], N. Tosi[a]

INFN Sezione di Catania[a], Università di Catania[b], Catania, Italy
S. Albergo[a,b], A. Di Mattia[a], R. Potenza[a,b], A. Tricomi[a,b], C. Tuve[a,b]

INFN Sezione di Firenze[a], Università di Firenze[b], Firenze, Italy
G. Barbagli[a], K. Chatterjee[a,b], V. Ciulli[a,b], C. Civinini[a], R. D'Alessandro[a,b], E. Focardi[a,b], G. Latino, P. Lenzi[a,b], M. Meschini[a], S. Paoletti[a], L. Russo[a,30], G. Sguazzoni[a], D. Strom[a], L. Viliani[a]

INFN Laboratori Nazionali di Frascati, Frascati, Italy
L. Benussi, S. Bianco, F. Fabbri, D. Piccolo

INFN Sezione di Genova[a], Università di Genova[b], Genoa, Italy
F. Ferro[a], R. Mulargia[a,b], E. Robutti[a], S. Tosi[a,b]

INFN Sezione di Milano-Bicocca[a], Università di Milano-Bicocca[b], Milan, Italy
A. Benaglia[a], A. Beschi[b], F. Brivio[a,b], V. Ciriolo[a,b,16], S. Di Guida[a,b,16], M. E. Dinardo[a,b], S. Fiorendi[a,b], S. Gennai[a], A. Ghezzi[a,b], P. Govoni[a,b], M. Malberti[a,b], S. Malvezzi[a], D. Menasce[a], F. Monti, L. Moroni[a], M. Paganoni[a,b], D. Pedrini[a], S. Ragazzi[a,b], T. Tabarelli de Fatis[a,b], D. Zuolo[a,b]

INFN Sezione di Napoli[a], Università di Napoli 'Federico II' [b], Napoli, Italy, Università della Basilicata[c], Potenza, Italy, Università G. Marconi[d], Rome, Italy
S. Buontempo[a], N. Cavallo[a,c], A. De Iorio[a,b], A. Di Crescenzo[a,b], F. Fabozzi[a,c], F. Fienga[a], G. Galati[a], A. O. M. Iorio[a,b], L. Lista[a], S. Meola[a,d,16], P. Paolucci[a,16], C. Sciacca[a,b], E. Voevodina[a,b]

INFN Sezione di Padova[a], Università di Padova[b], Padova, Italy, Università di Trento[c], Trento, Italy
P. Azzi[a], N. Bacchetta[a], D. Bisello[a,b], A. Boletti[a,b], A. Bragagnolo, R. Carlin[a,b], P. Checchia[a], M. Dall'Osso[a,b], P. De Castro Manzano[a], T. Dorigo[a], U. Dosselli[a], F. Gasparini[a,b], U. Gasparini[a,b], A. Gozzelino[a], S. Y. Hoh, S. Lacaprara[a], P. Lujan, M. Margoni[a,b], A. T. Meneguzzo[a,b], J. Pazzini[a,b], M. Presilla[b], P. Ronchese[a,b], R. Rossin[a,b], F. Simonetto[a,b], A. Tiko, E. Torassa[a], M. Tosi[a,b], M. Zanetti[a,b], P. Zotto[a,b], G. Zumerle[a,b]

INFN Sezione di Pavia[a], Università di Pavia[b], Pavia, Italy
A. Braghieri[a], A. Magnani[a], P. Montagna[a,b], S. P. Ratti[a,b], V. Re[a], M. Ressegotti[a,b], C. Riccardi[a,b], P. Salvini[a], I. Vai[a,b], P. Vitulo[a,b]

INFN Sezione di Perugia[a], Università di Perugia[b], Perugia, Italy
M. Biasini[a,b], G. M. Bilei[a], C. Cecchi[a,b], D. Ciangottini[a,b], L. Fanò[a,b], P. Lariccia[a,b], R. Leonardi[a,b], E. Manoni[a], G. Mantovani[a,b], V. Mariani[a,b], M. Menichelli[a], A. Rossi[a,b], A. Santocchia[a,b], D. Spiga[a]

INFN Sezione di Pisa[a], Università di Pisa[b], Scuola Normale Superiore di Pisa[c], Pisa, Italy
K. Androsov[a], P. Azzurri[a], G. Bagliesi[a], L. Bianchini[a], T. Boccali[a], L. Borrello, R. Castaldi[a], M. A. Ciocci[a,b], R. Dell'Orso[a], G. Fedi[a], F. Fiori[a,c], L. Giannini[a,c], A. Giassi[a], M. T. Grippo[a], F. Ligabue[a,c], E. Manca[a,c], G. Mandorli[a,c], A. Messineo[a,b], F. Palla[a], A. Rizzi[a,b], G. Rolandi[31], P. Spagnolo[a], R. Tenchini[a], G. Tonelli[a,b], A. Venturi[a], P. G. Verdini[a]

INFN Sezione di Roma[a], Sapienza Università di Roma[b], Rome, Italy
L. Barone[a,b], F. Cavallari[a], M. Cipriani[a,b], D. Del Re[a,b], E. Di Marco[a,b], M. Diemoz[a], S. Gelli[a,b], E. Longo[a,b], B. Marzocchi[a,b], P. Meridiani[a], G. Organtini[a,b], F. Pandolfi[a], R. Paramatti[a,b], F. Preiato[a,b], S. Rahatlou[a,b], C. Rovelli[a], F. Santanastasio[a,b]

INFN Sezione di Torino[a], Università di Torino[b], Torino, Italy, Università del Piemonte Orientale[c], Novara, Italy
N. Amapane[a,b], R. Arcidiacono[a,c], S. Argiro[a,b], M. Arneodo[a,c], N. Bartosik[a], R. Bellan[a,b], C. Biino[a], A. Cappati[a,b], N. Cartiglia[a], F. Cenna[a,b], S. Cometti[a], M. Costa[a,b], R. Covarelli[a,b], N. Demaria[a], B. Kiani[a,b], C. Mariotti[a], S. Maselli[a], E. Migliore[a,b], V. Monaco[a,b], E. Monteil[a,b], M. Monteno[a], M. M. Obertino[a,b], L. Pacher[a,b], N. Pastrone[a], M. Pelliccioni[a], G. L. Pinna Angioni[a,b], A. Romero[a,b], M. Ruspa[a,c], R. Sacchi[a,b], R. Salvatico[a,b], K. Shchelina[a,b], V. Sola[a], A. Solano[a,b], D. Soldi[a,b], A. Staiano[a]

INFN Sezione di Trieste[a], Università di Trieste[b], Trieste, Italy
S. Belforte[a], V. Candelise[a,b], M. Casarsa[a], F. Cossutti[a], A. Da Rold[a,b], G. Della Ricca[a,b], F. Vazzoler[a,b], A. Zanetti[a]

Kyungpook National University, Daegu, Korea
D. H. Kim, G. N. Kim, M. S. Kim, J. Lee, S. Lee, S. W. Lee, C. S. Moon, Y. D. Oh, S. I. Pak, S. Sekmen, D. C. Son, Y. C. Yang

Chonnam National University, Institute for Universe and Elementary Particles, Kwangju, Korea
H. Kim, D. H. Moon, G. Oh

Hanyang University, Seoul, Korea
B. Francois, J. Goh[32], T. J. Kim

Korea University, Seoul, Korea
S. Cho, S. Choi, Y. Go, D. Gyun, S. Ha, B. Hong, Y. Jo, K. Lee, K. S. Lee, S. Lee, J. Lim, S. K. Park, Y. Roh

Sejong University, Seoul, Korea
H. S. Kim

Seoul National University, Seoul, Korea
J. Almond, J. Kim, J. S. Kim, H. Lee, K. Lee, K. Nam, S. B. Oh, B. C. Radburn-Smith, S. h. Seo, U. K. Yang, H. D. Yoo, G. B. Yu

University of Seoul, Seoul, Korea
D. Jeon, H. Kim, J. H. Kim, J. S. H. Lee, I. C. Park

Sungkyunkwan University, Suwon, Korea
Y. Choi, C. Hwang, J. Lee, I. Yu

Riga Technical University, Riga, Latvia
V. Veckalns[33]

Vilnius University, Vilnius, Lithuania
V. Dudenas, A. Juodagalvis, J. Vaitkus

National Centre for Particle Physics, Universiti Malaya, Kuala Lumpur, Malaysia
Z. A. Ibrahim, M. A. B. Md Ali[34], F. Mohamad Idris[35], W. A. T. Wan Abdullah, M. N. Yusli, Z. Zolkapli

Universidad de Sonora (UNISON), Hermosillo, Mexico
J. F. Benitez, A. Castaneda Hernandez, J. A. Murillo Quijada

Centro de Investigacion y de Estudios Avanzados del IPN, Mexico City, Mexico
H. Castilla-Valdez, E. De La Cruz-Burelo, M. C. Duran-Osuna, I. Heredia-De La Cruz[36], R. Lopez-Fernandez, J. Mejia Guisao, R. I. Rabadan-Trejo, M. Ramirez-Garcia, G. Ramirez-Sanchez, R. Reyes-Almanza, A. Sanchez-Hernandez

Universidad Iberoamericana, Mexico City, Mexico
S. Carrillo Moreno, C. Oropeza Barrera, F. Vazquez Valencia

Benemerita Universidad Autonoma de Puebla, Puebla, Mexico
J. Eysermans, I. Pedraza, H. A. Salazar Ibarguen, C. Uribe Estrada

Universidad Autónoma de San Luis Potosí, San Luis Potosí, Mexico
A. Morelos Pineda

University of Auckland, Auckland, New Zealand
D. Krofcheck

University of Canterbury, Christchurch, New Zealand
S. Bheesette, P. H. Butler

National Centre for Physics, Quaid-I-Azam University, Islamabad, Pakistan
A. Ahmad, M. Ahmad, M. I. Asghar, Q. Hassan, H. R. Hoorani, W. A. Khan, M. A. Shah, M. Shoaib, M. Waqas

National Centre for Nuclear Research, Swierk, Poland
H. Bialkowska, M. Bluj, B. Boimska, T. Frueboes, M. Górski, M. Kazana, M. Szleper, P. Traczyk, P. Zalewski

Institute of Experimental Physics, Faculty of Physics, University of Warsaw, Warsaw, Poland
K. Bunkowski, A. Byszuk[37], K. Doroba, A. Kalinowski, M. Konecki, J. Krolikowski, M. Misiura, M. Olszewski, A. Pyskir, M. Walczak

Laboratório de Instrumentação e Física Experimental de Partículas, Lisbon, Portugal
M. Araujo, P. Bargassa, C. Beirão Da Cruz E Silva, A. Di Francesco, P. Faccioli, B. Galinhas, M. Gallinaro, J. Hollar, N. Leonardo, J. Seixas, G. Strong, O. Toldaiev, J. Varela

Joint Institute for Nuclear Research, Dubna, Russia
S. Afanasiev, P. Bunin, M. Gavrilenko, I. Golutvin, I. Gorbunov, A. Kamenev, V. Karjavine, A. Lanev, A. Malakhov, V. Matveev[38,39], P. Moisenz, V. Palichik, V. Perelygin, S. Shmatov, S. Shulha, N. Skatchkov, V. Smirnov, N. Voytishin, A. Zarubin

Petersburg Nuclear Physics Institute, Gatchina, St. Petersburg, Russia
V. Golovtsov, Y. Ivanov, V. Kim[40], E. Kuznetsova[41], P. Levchenko, V. Murzin, V. Oreshkin, I. Smirnov, D. Sosnov, V. Sulimov, L. Uvarov, S. Vavilov, A. Vorobyev

Institute for Nuclear Research, Moscow, Russia
Yu. Andreev, A. Dermenev, S. Gninenko, N. Golubev, A. Karneyeu, M. Kirsanov, N. Krasnikov, A. Pashenkov, A. Shabanov, D. Tlisov, A. Toropin

Institute for Theoretical and Experimental Physics, Moscow, Russia
V. Epshteyn, V. Gavrilov, N. Lychkovskaya, V. Popov, I. Pozdnyakov, G. Safronov, A. Spiridonov, A. Stepennov, V. Stolin, M. Toms, E. Vlasov, A. Zhokin

Moscow Institute of Physics and Technology, Moscow, Russia
T. Aushev

National Research Nuclear University 'Moscow Engineering Physics Institute' (MEPhI), Moscow, Russia
R. Chistov[42], M. Danilov[42], P. Parygin, E. Tarkovskii

P.N. Lebedev Physical Institute, Moscow, Russia
V. Andreev, M. Azarkin, I. Dremin[39], M. Kirakosyan, A. Terkulov

Skobeltsyn Institute of Nuclear Physics, Lomonosov Moscow State University, Moscow, Russia
A. Baskakov, A. Belyaev, E. Boos, V. Bunichev, M. Dubinin[43], L. Dudko, V. Klyukhin, N. Korneeva, I. Lokhtin, S. Obraztsov, M. Perfilov, V. Savrin, P. Volkov

Novosibirsk State University (NSU), Novosibirsk, Russia
A. Barnyakov[44], V. Blinov[44], T. Dimova[44], L. Kardapoltsev[44], Y. Skovpen[44]

Institute for High Energy Physics of National Research Centre 'Kurchatov Institute', Protvino, Russia
I. Azhgirey, I. Bayshev, S. Bitioukov, V. Kachanov, A. Kalinin, D. Konstantinov, P. Mandrik, V. Petrov, R. Ryutin, S. Slabospitskii, A. Sobol, S. Troshin, N. Tyurin, A. Uzunian, A. Volkov

National Research Tomsk Polytechnic University, Tomsk, Russia
A. Babaev, S. Baidali, V. Okhotnikov

Faculty of Physics and Vinca Institute of Nuclear Sciences, University of Belgrade, Belgrade, Serbia
P. Adzic[45], P. Cirkovic, D. Devetak, M. Dordevic, P. Milenovic[46], J. Milosevic

Centro de Investigaciones Energéticas Medioambientales y Tecnológicas (CIEMAT), Madrid, Spain
J. Alcaraz Maestre, A. Álvarez Fernández, I. Bachiller, M. Barrio Luna, J. A. Brochero Cifuentes, M. Cerrada, N. Colino, B. De La Cruz, A. Delgado Peris, C. Fernandez Bedoya, J. P. Fernández Ramos, J. Flix, M. C. Fouz, O. Gonzalez Lopez, S. Goy Lopez, J. M. Hernandez, M. I. Josa, D. Moran, A. Pérez-Calero Yzquierdo, J. Puerta Pelayo, I. Redondo, L. Romero, S. Sánchez Navas, M. S. Soares, A. Triossi

Universidad Autónoma de Madrid, Madrid, Spain
C. Albajar, J. F. de Trocóniz

Universidad de Oviedo, Oviedo, Spain
J. Cuevas, C. Erice, J. Fernandez Menendez, S. Folgueras, I. Gonzalez Caballero, J. R. González Fernández, E. Palencia Cortezon, V. Rodríguez Bouza, S. Sanchez Cruz, J. M. Vizan Garcia

Instituto de Física de Cantabria (IFCA), CSIC-Universidad de Cantabria, Santander, Spain
I. J. Cabrillo, A. Calderon, B. Chazin Quero, J. Duarte Campderros, M. Fernandez, P. J. Fernández Manteca, A. García Alonso, J. Garcia-Ferrero, G. Gomez, A. Lopez Virto, J. Marco, C. Martinez Rivero, P. Martinez Ruiz del Arbol, F. Matorras, J. Piedra Gomez, C. Prieels, T. Rodrigo, A. Ruiz-Jimeno, L. Scodellaro, N. Trevisani, I. Vila, R. Vilar Cortabitarte

Department of Physics, University of Ruhuna, Matara, Sri Lanka
N. Wickramage

CERN, European Organization for Nuclear Research, Geneva, Switzerland
D. Abbaneo, B. Akgun, E. Auffray, G. Auzinger, P. Baillon, A. H. Ball, D. Barney, J. Bendavid, M. Bianco, A. Bocci, C. Botta, E. Brondolin, T. Camporesi, M. Cepeda, G. Cerminara, E. Chapon, Y. Chen, G. Cucciati, D. d'Enterria, A. Dabrowski, N. Daci, V. Daponte, A. David, A. De Roeck, N. Deelen, M. Dobson, M. Dünser, N. Dupont, A. Elliott-Peisert, F. Fallavollita[47], D. Fasanella, G. Franzoni, J. Fulcher, W. Funk, D. Gigi, A. Gilbert, K. Gill, F. Glege, M. Gruchala, M. Guilbaud, D. Gulhan, J. Hegeman, C. Heidegger, V. Innocente, G. M. Innocenti, A. Jafari, P. Janot, O. Karacheban[19], J. Kieseler, A. Kornmayer, M. Krammer[1], C. Lange, P. Lecoq, C. Lourenço, L. Malgeri, M. Mannelli, A. Massironi, F. Meijers, J. A. Merlin, S. Mersi, E. Meschi, F. Moortgat, M. Mulders, J. Ngadiuba, S. Nourbakhsh, S. Orfanelli, L. Orsini, F. Pantaleo[16], L. Pape, E. Perez, M. Peruzzi, A. Petrilli, G. Petrucciani, A. Pfeiffer, M. Pierini, F. M. Pitters, D. Rabady, A. Racz, M. Rovere, H. Sakulin, C. Schäfer, C. Schwick, M. Selvaggi, A. Sharma, P. Silva, P. Sphicas[48], A. Stakia, J. Steggemann, D. Treille, A. Tsirou, A. Vartak, M. Verzetti, W. D. Zeuner

Paul Scherrer Institut, Villigen, Switzerland
L. Caminada[49], K. Deiters, W. Erdmann, R. Horisberger, Q. Ingram, H. C. Kaestli, D. Kotlinski, U. Langenegger, T. Rohe, S. A. Wiederkehr

ETH Zurich-Institute for Particle Physics and Astrophysics (IPA), Zurich, Switzerland
M. Backhaus, L. Bäni, P. Berger, N. Chernyavskaya, G. Dissertori, M. Dittmar, M. Donegà, C. Dorfer, T. A. Gómez Espinosa, C. Grab, D. Hits, T. Klijnsma, W. Lustermann, R. A. Manzoni, M. Marionneau, M. T. Meinhard, F. Micheli, P. Musella, F. Nessi-Tedaldi, F. Pauss, G. Perrin, L. Perrozzi, S. Pigazzini, M. Reichmann, C. Reissel, D. Ruini, D. A. Sanz Becerra, M. Schönenberger, L. Shchutska, V. R. Tavolaro, K. Theofilatos, M. L. Vesterbacka Olsson, R. Wallny, D. H. Zhu

Universität Zürich, Zurich, Switzerland
T. K. Aarrestad, C. Amsler[50], D. Brzhechko, M. F. Canelli, A. De Cosa, R. Del Burgo, S. Donato, C. Galloni, T. Hreus, B. Kilminster, S. Leontsinis, I. Neutelings, G. Rauco, P. Robmann, D. Salerno, K. Schweiger, C. Seitz, Y. Takahashi, A. Zucchetta

National Central University, Chung-Li, Taiwan
T. H. Doan, R. Khurana, C. M. Kuo, W. Lin, S. S. Yu

National Taiwan University (NTU), Taipei, Taiwan
P. Chang, Y. Chao, K. F. Chen, P. H. Chen, W.-S. Hou, Y. F. Liu, R.-S. Lu, E. Paganis, A. Psallidas, A. Steen

Department of Physics, Faculty of Science, Chulalongkorn University, Bangkok, Thailand
B. Asavapibhop, N. Srimanobhas, N. Suwonjandee

Physics Department, Science and Art Faculty, Çukurova University, Adana, Turkey
A. Bat, F. Boran, S. Cerci[51], S. Damarseckin, Z. S. Demiroglu, F. Dolek, C. Dozen, I. Dumanoglu, G. Gokbulut, Y. Guler, E. Gurpinar, I. Hos[52], C. Isik, E. E. Kangal[53], O. Kara, A. Kayis Topaksu, U. Kiminsu, M. Oglakci, G. Onengut, K. Ozdemir[54], S. Ozturk[55], D. Sunar Cerci[51], B. Tali[51], U. G. Tok, S. Turkcapar, I. S. Zorbakir, C. Zorbilmez

Physics Department, Middle East Technical University, Ankara, Turkey
B. Isildak[56], G. Karapinar[57], M. Yalvac, M. Zeyrek

Bogazici University, Istanbul, Turkey
I. O. Atakisi, E. Gülmez, M. Kaya[58], O. Kaya[59], S. Ozkorucuklu[60], S. Tekten, E. A. Yetkin[61]

Istanbul Technical University, Istanbul, Turkey
M. N. Agaras, A. Cakir, K. Cankocak, Y. Komurcu, S. Sen[62]

Institute for Scintillation Materials of National Academy of Science of Ukraine, Kharkov, Ukraine
B. Grynyov

National Scientific Center, Kharkov Institute of Physics and Technology, Kharkov, Ukraine
L. Levchuk

University of Bristol, Bristol, UK
F. Ball, J. J. Brooke, D. Burns, E. Clement, D. Cussans, O. Davignon, H. Flacher, J. Goldstein, G. P. Heath, H. F. Heath, L. Kreczko, D. M. Newbold[63], S. Paramesvaran, B. Penning, T. Sakuma, D. Smith, V. J. Smith, J. Taylor, A. Titterton

Rutherford Appleton Laboratory, Didcot, UK
K. W. Bell, A. Belyaev[64], C. Brew, R. M. Brown, D. Cieri, D. J. A. Cockerill, J. A. Coughlan, K. Harder, S. Harper, J. Linacre, K. Manolopoulos, E. Olaiya, D. Petyt, T. Reis, T. Schuh, C. H. Shepherd-Themistocleous, A. Thea, I. R. Tomalin, T. Williams, W. J. Womersley

Imperial College, London, UK
R. Bainbridge, P. Bloch, J. Borg, S. Breeze, O. Buchmuller, A. Bundock, D. Colling, P. Dauncey, G. Davies, M. Della Negra, R. Di Maria, P. Everaerts, G. Hall, G. Iles, T. James, M. Komm, C. Laner, L. Lyons, A.-M. Magnan, S. Malik, A. Martelli, J. Nash[65], A. Nikitenko[7], V. Palladino, M. Pesaresi, D. M. Raymond, A. Richards, A. Rose, E. Scott, C. Seez, A. Shtipliyski, G. Singh, M. Stoye, T. Strebler, S. Summers, A. Tapper, K. Uchida, T. Virdee[16], N. Wardle, D. Winterbottom, J. Wright, S. C. Zenz

Brunel University, Uxbridge, UK
J. E. Cole, P. R. Hobson, A. Khan, P. Kyberd, C. K. Mackay, A. Morton, I. D. Reid, L. Teodorescu, S. Zahid

Baylor University, Waco, USA
K. Call, J. Dittmann, K. Hatakeyama, H. Liu, C. Madrid, B. McMaster, N. Pastika, C. Smith

Catholic University of America, Washington, DC, USA
R. Bartek, A. Dominguez

The University of Alabama, Tuscaloosa, USA
A. Buccilli, S. I. Cooper, C. Henderson, P. Rumerio, C. West

Boston University, Boston, USA
D. Arcaro, T. Bose, Z. Demiragli, D. Gastler, S. Girgis, D. Pinna, C. Richardson, J. Rohlf, D. Sperka, I. Suarez, L. Sulak, D. Zou

Brown University, Providence, USA
G. Benelli, B. Burkle, X. Coubez, D. Cutts, M. Hadley, J. Hakala, U. Heintz, J. M. Hogan[66], K. H. M. Kwok, E. Laird, G. Landsberg, J. Lee, Z. Mao, M. Narain, S. Sagir[67], R. Syarif, E. Usai, D. Yu

University of California, Davis, Davis, USA
R. Band, C. Brainerd, R. Breedon, D. Burns, M. Calderon De La Barca Sanchez, M. Chertok, J. Conway, R. Conway, P. T. Cox, R. Erbacher, C. Flores, G. Funk, W. Ko, O. Kukral, R. Lander, M. Mulhearn, D. Pellett, J. Pilot, S. Shalhout, M. Shi, D. Stolp, D. Taylor, K. Tos, M. Tripathi, Z. Wang, F. Zhang

University of California, Los Angeles, USA
M. Bachtis, C. Bravo, R. Cousins, A. Dasgupta, S Erhan, A. Florent, J. Hauser, M. Ignatenko, N. Mccoll, S. Regnard, D. Saltzberg, C. Schnaible, V. Valuev

University of California, Riverside, Riverside, USA
E. Bouvier, K. Burt, R. Clare, J. W. Gary, S. M. A. Ghiasi Shirazi, G. Hanson, G. Karapostoli, E. Kennedy, F. Lacroix, O. R. Long, M. Olmedo Negrete, M. I. Paneva, W. Si, L. Wang, H. Wei, S. Wimpenny, B. R. Yates

University of California, San Diego, La Jolla, USA
J. G. Branson, P. Chang, S. Cittolin, M. Derdzinski, R. Gerosa, D. Gilbert, B. Hashemi, A. Holzner, D. Klein, G. Kole, V. Krutelyov, J. Letts, M. Masciovecchio, S. May, D. Olivito, S. Padhi, M. Pieri, V. Sharma, M. Tadel, J. Wood, F. Würthwein, A. Yagil, G. Zevi Della Porta

Department of Physics, University of California, Santa Barbara, Santa Barbara, USA
N. Amin, R. Bhandari, C. Campagnari, M. Citron, V. Dutta, M. Franco Sevilla, L. Gouskos, R. Heller, J. Incandela, H. Mei, A. Ovcharova, H. Qu, J. Richman, D. Stuart, S. Wang, J. Yoo

California Institute of Technology, Pasadena, USA
D. Anderson, A. Bornheim, J. M. Lawhorn, N. Lu, H. B. Newman, T. Q. Nguyen, J. Pata, M. Spiropulu, J. R. Vlimant, R. Wilkinson, S. Xie, Z. Zhang, R. Y. Zhu

Carnegie Mellon University, Pittsburgh, USA
M. B. Andrews, T. Ferguson, T. Mudh olkar, M. Paulini, M. Sun, I. Vorobiev, M. Weinberg

University of Colorado Boulder, Boulder, USA
J. P. Cumalat, W. T. Ford, F. Jensen, A. Johnson, E. MacDonald, T. Mulholland, R. Patel, A. Perloff, K. Stenson, K. A. Ulmer, S. R. Wagner

Cornell University, Ithaca, USA
J. Alexander, J. Chaves, Y. Cheng, J. Chu, A. Datta, K. Mcdermott, N. Mirman, J. R. Patterson, D. Quach, A. Rinkevicius, A. Ryd, L. Skinnari, L. Soffi, S. M. Tan, Z. Tao, J. Thom, J. Tucker, P. Wittich, M. Zientek

Fermi National Accelerator Laboratory, Batavia, USA
S. Abdullin, M. Albrow, M. Alyari, G. Apollinari, A. Apresyan, A. Apyan, S. Banerjee, L. A. T. Bauerdick, A. Beretvas, J. Berryhill, P. C. Bhat, K. Burkett, J. N. Butler, A. Canepa, G. B. Cerati, H. W. K. Cheung, F. Chlebana, M. Cremonesi, J. Duarte, V. D. Elvira, J. Freeman, Z. Gecse, E. Gottschalk, L. Gray, D. Green, S. Grünendahl, O. Gutsche, J. Hanlon, R. M. Harris, S. Hasegawa, J. Hirschauer, Z. Hu, B. Jayatilaka, S. Jindariani, M. Johnson, U. Joshi, B. Klima, M. J. Kortelainen, B. Kreis, S. Lammel, D. Lincoln, R. Lipton, M. Liu, T. Liu, J. Lykken, K. Maeshima, J. M. Marraffino, D. Mason, P. McBride, P. Merkel, S. Mrenna, S. Nahn, V. O'Dell, K. Pedro, C. Pena, O. Prokofyev, G. Rakness, F. Ravera, A. Reinsvold, L. Ristori, A. Savoy-Navarro[68], B. Schneider, E. Sexton-Kennedy, A. Soha, W. J. Spalding, L. Spiegel, S. Stoynev, J. Strait, N. Strobbe, L. Taylor, S. Tkaczyk, N. V. Tran, L. Uplegger, E. W. Vaandering, C. Vernieri, M. Verzocchi, R. Vidal, M. Wang, H. A. Weber

University of Florida, Gainesville, USA
D. Acosta, P. Avery, P. Bortignon, D. Bourilkov, A. Brinkerhoff, L. Cadamuro, A. Carnes, D. Curry, R. D. Field, S. V. Gleyzer, B. M. Joshi, J. Konigsberg, A. Korytov, K. H. Lo, P. Ma, K. Matchev, N. Menendez, G. Mitselmakher, D. Rosenzweig, K. Shi, J. Wang, S. Wang, X. Zuo

Florida International University, Miami, USA
Y. R. Joshi, S. Linn

Florida State University, Tallahassee, USA
A. Ackert, T. Adams, A. Askew, S. Hagopian, V. Hagopian, K. F. Johnson, T. Kolberg, G. Martinez, T. Perry, H. Prosper, A. Saha, C. Schiber, R. Yohay

Florida Institute of Technology, Melbourne, USA
M. M. Baarmand, V. Bhopatkar, S. Colafranceschi, M. Hohlmann, D. Noonan, M. Rahmani, T. Roy, M. Saunders, F. Yumiceva

University of Illinois at Chicago (UIC), Chicago, USA
M. R. Adams, L. Apanasevich, D. Berry, R. R. Betts, R. Cavanaugh, X. Chen, S. Dittmer, O. Evdokimov, C. E. Gerber, D. A. Hangal, D. J. Hofman, K. Jung, J. Kamin, C. Mills, M. B. Tonjes, N. Varelas, H. Wang, X. Wang, Z. Wu, J. Zhang

The University of Iowa, Iowa City, USA
M. Alhusseini, B. Bilki[69], W. Clarida, K. Dilsiz[70], S. Durgut, R. P. Gandrajula, M. Haytmyradov, V. Khristenko, J.-P. Merlo, A. Mestvirishvili, A. Moeller, J. Nachtman, H. Ogul[71], Y. Onel, F. Ozok[72], A. Penzo, C. Snyder, E. Tiras, J. Wetzel

Johns Hopkins University, Baltimore, USA
B. Blumenfeld, A. Cocoros, N. Eminizer, D. Fehling, L. Feng, A. V. Gritsan, W. T. Hung, P. Maksimovic, J. Roskes, U. Sarica, M. Swartz, M. Xiao

The University of Kansas, Lawrence, USA
A. Al-bataineh, P. Baringer, A. Bean, S. Boren, J. Bowen, A. Bylinkin, J. Castle, S. Khalil, A. Kropivnitskaya, D. Majumder, W. Mcbrayer, M. Murray, C. Rogan, S. Sanders, E. Schmitz, J. D. Tapia Takaki, Q. Wang

Kansas State University, Manhattan, USA
S. Duric, A. Ivanov, K. Kaadze, D. Kim, Y. Maravin, D. R. Mendis, T. Mitchell, A. Modak, A. Mohammadi

Lawrence Livermore National Laboratory, Livermore, USA
F. Rebassoo, D. Wright

University of Maryland, College Park, USA
A. Baden, O. Baron, A. Belloni, S. C. Eno, Y. Feng, C. Ferraioli, N. J. Hadley, S. Jabeen, G. Y. Jeng, R. G. Kellogg, J. Kunkle, A. C. Mignerey, S. Nabili, F. Ricci-Tam, M. Seidel, Y. H. Shin, A. Skuja, S. C. Tonwar, K. Wong

Massachusetts Institute of Technology, Cambridge, USA
D. Abercrombie, B. Allen, V. Azzolini, A. Baty, R. Bi, S. Brandt, W. Busza, I. A. Cali, M. D'Alfonso, G. Gomez Ceballos, M. Goncharov, P. Harris, D. Hsu, M. Hu, Y. Iiyama, M. Klute, D. Kovalskyi, Y.-J. Lee, P. D. Luckey, B. Maier, A. C. Marini, C. Mcginn, C. Mironov, S. Narayanan, X. Niu, C. Paus, D. Rankin, C. Roland, G. Roland, Z. Shi, G. S. F. Stephans, K. Sumorok, K. Tatar, D. Velicanu, J. Wang, T. W. Wang, B. Wyslouch

University of Minnesota, Minneapolis, USA
A. C. Benvenuti[†], R. M. Chatterjee, A. Evans, P. Hansen, J. Hiltbrand, Sh. Jain, S. Kalafut, M. Krohn, Y. Kubota, Z. Lesko, J. Mans, R. Rusack, M. A. Wadud

University of Mississippi, Oxford, USA
J. G. Acosta, S. Oliveros

University of Nebraska-Lincoln, Lincoln, USA
E. Avdeeva, K. Bloom, D. R. Claes, C. Fangmeier, F. Golf, R. Gonzalez Suarez, R. Kamalieddin, I. Kravchenko, J. Monroy, J. E. Siado, G. R. Snow, B. Stieger

State University of New York at Buffalo, Buffalo, USA
A. Godshalk, C. Harrington, I. Iashvili, A. Kharchilava, C. Mclean, D. Nguyen, A. Parker, S. Rappoccio, B. Roozbahani

Northeastern University, Boston, USA
G. Alverson, E. Barberis, C. Freer, Y. Haddad, A. Hortiangtham, G. Madigan, D. M. Morse, T. Orimoto, A. Tishelman-charny, T. Wamorkar, B. Wang, A. Wisecarver, D. Wood

Northwestern University, Evanston, USA
S. Bhattacharya, J. Bueghly, O. Charaf, T. Gunter, K. A. Hahn, N. Odell, M. H. Schmitt, K. Sung, M. Trovato, M. Velasco

University of Notre Dame, Notre Dame, USA
R. Bucci, N. Dev, R. Goldouzian, M. Hildreth, K. Hurtado Anampa, C. Jessop, D. J. Karmgard, K. Lannon, W. Li, N. Loukas, N. Marinelli, F. Meng, C. Mueller, Y. Musienko[38], M. Planer, R. Ruchti, P. Siddireddy, G. Smith, S. Taroni, M. Wayne, A. Wightman, M. Wolf, A. Woodard

The Ohio State University, Columbus, USA
J. Alimena, L. Antonelli, B. Bylsma, L. S. Durkin, S. Flowers, B. Francis, C. Hill, W. Ji, T. Y. Ling, W. Luo, B. L. Winer

Princeton University, Princeton, USA
S. Cooperstein, G. Dezoort, P. Elmer, J. Hardenbrook, N. Haubrich, S. Higginbotham, A. Kalogeropoulos, S. Kwan, D. Lange, M. T. Lucchini, J. Luo, D. Marlow, K. Mei, I. Ojalvo, J. Olsen, C. Palmer, P. Piroué, J. Salfeld-Nebgen, D. Stickland, C. Tully

University of Puerto Rico, Mayaguez, USA
S. Malik, S. Norberg

Purdue University, West Lafayette, USA
A. Barker, V. E. Barnes, S. Das, L. Gutay, M. Jones, A. W. Jung, A. Khatiwada, B. Mahakud, D. H. Miller, N. Neumeister, C. C. Peng, S. Piperov, H. Qiu, J. F. Schulte, J. Sun, F. Wang, R. Xiao, W. Xie

Purdue University Northwest, Hammond, USA
T. Cheng, J. Dolen, N. Parashar

Rice University, Houston, USA
Z. Chen, K. M. Ecklund, S. Freed, F. J. M. Geurts, M. Kilpatrick, Arun Kumar, W. Li, B. P. Padley, R. Redjimi, J. Roberts, J. Rorie, W. Shi, Z. Tu, A. Zhang

University of Rochester, Rochester, USA
A. Bodek, P. de Barbaro, R. Demina, Y. t. Duh, J. L. Dulemba, C. Fallon, T. Ferbel, M. Galanti, A. Garcia-Bellido, J. Han, O. Hindrichs, A. Khukhunaishvili, E. Ranken, P. Tan, R. Taus

Rutgers, The State University of New Jersey, Piscataway, USA
B. Chiarito, J. P. Chou, Y. Gershtein, E. Halkiadakis, A. Hart, M. Heindl, E. Hughes, S. Kaplan, R. Kunnawalkam Elayavalli, S. Kyriacou, I. Laflotte, A. Lath, R. Montalvo, K. Nash, M. Osherson, H. Saka, S. Salur, S. Schnetzer, D. Sheffield, S. Somalwar, R. Stone, S. Thomas, P. Thomassen

University of Tennessee, Knoxville, USA
H. Acharya, A. G. Delannoy, J. Heideman, G. Riley, S. Spanier

Texas A&M University, College Station, USA
O. Bouhali[73], A. Celik, M. Dalchenko, M. De Mattia, A. Delgado, S. Dildick, R. Eusebi, J. Gilmore, T. Huang, T. Kamon[74], S. Luo, D. Marley, R. Mueller, D. Overton, L. Perniè, D. Rathjens, A. Safonov

Texas Tech University, Lubbock, USA
N. Akchurin, J. Damgov, F. De Guio, P. R. Dudero, S. Kunori, K. Lamichhane, S. W. Lee, T. Mengke, S. Muthumuni, T. Peltola, S. Undleeb, I. Volobouev, Z. Wang, A. Whitbeck

Vanderbilt University, Nashville, USA
S. Greene, A. Gurrola, R. Janjam, W. Johns, C. Maguire, A. Melo, H. Ni, K. Padeken, F. Romeo, P. Sheldon, S. Tuo, J. Velkovska, M. Verweij, Q. Xu

University of Virginia, Charlottesville, USA
M. W. Arenton, P. Barria, B. Cox, R. Hirosky, M. Joyce, A. Ledovskoy, H. Li, C. Neu, T. Sinthuprasith, Y. Wang, E. Wolfe, F. Xia

Wayne State University, Detroit, USA
R. Harr, P. E. Karchin, N. Poudyal, J. Sturdy, P. Thapa, S. Zaleski

University of Wisconsin-Madison, Madison, WI, USA
J. Buchanan, C. Caillol, D. Carlsmith, S. Dasu, I. De Bruyn, L. Dodd, B. Gomber[75], M. Grothe, M. Herndon, A. Hervé, U. Hussain, P. Klabbers, A. Lanaro, K. Long, R. Loveless, T. Ruggles, A. Savin, V. Sharma, N. Smith, W. H. Smith, N. Woods

† **Deceased**

1: Also at Vienna University of Technology, Vienna, Austria
2: Also at IRFU, CEA, Université Paris-Saclay, Gif-sur-Yvette, France
3: Also at Universidade Estadual de Campinas, Campinas, Brazil
4: Also at Federal University of Rio Grande do Sul, Porto Alegre, Brazil
5: Also at Université Libre de Bruxelles, Brussels, Belgium
6: Also at University of Chinese Academy of Sciences, Beijing, China
7: Also at Institute for Theoretical and Experimental Physics, Moscow, Russia
8: Also at Joint Institute for Nuclear Research, Dubna, Russia
9: Also at Cairo University, Cairo, Egypt
10: Also at Zewail City of Science and Technology, Zewail, Egypt
11: Also at British University in Egypt, Cairo Egypt
12: Now at Ain Shams University, Cairo, Egypt
13: Also at Department of Physics, King Abdulaziz University, Jeddah, Saudi Arabia
14: Also at Université de Haute Alsace, Mulhouse, France
15: Also at Skobeltsyn Institute of Nuclear Physics, Lomonosov Moscow State University, Moscow, Russia
16: Also at CERN, European Organization for Nuclear Research, Geneva, Switzerland
17: Also at RWTH Aachen University, III. Physikalisches Institut A, Aachen, Germany
18: Also at University of Hamburg, Hamburg, Germany
19: Also at Brandenburg University of Technology, Cottbus, Germany
20: Also at Institute of Physics, University of Debrecen, Debrecen, Hungary
21: Also at Institute of Nuclear Research ATOMKI, Debrecen, Hungary
22: Also at MTA-ELTE Lendület CMS Particle and Nuclear Physics Group, Eötvös Loránd University, Budapest, Hungary
23: Also at Indian Institute of Technology Bhubaneswar, Bhubaneswar, India
24: Also at Institute of Physics, Bhubaneswar, India
25: Also at Shoolini University, Solan, India
26: Also at University of Visva-Bharati, Santiniketan, India
27: Also at Isfahan University of Technology, Isfahan, Iran
28: Also at Plasma Physics Research Center, Science and Research Branch, Islamic Azad University, Tehran, Iran
29: Also at ITALIAN NATIONAL AGENCY FOR NEW TECHNOLOGIES, ENERGY AND SUSTAINABLE ECONOMIC DEVELOPMENT, Bologna, Italy
30: Also at Università degli Studi di Siena, Siena, Italy
31: Also at Scuola Normale e Sezione dell'INFN, Pisa, Italy
32: Also at Kyunghee University, Seoul, Korea
33: Also at Riga Technical University, Riga, Latvia
34: Also at International Islamic University of Malaysia, Kuala Lumpur, Malaysia
35: Also at Malaysian Nuclear Agency, MOSTI, Kajang, Malaysia
36: Also at Consejo Nacional de Ciencia y Tecnología, Mexico City, Mexico
37: Also at Warsaw University of Technology, Institute of Electronic Systems, Warsaw, Poland
38: Also at Institute for Nuclear Research, Moscow, Russia
39: Now at National Research Nuclear University 'Moscow Engineering Physics Institute' (MEPhI), Moscow, Russia
40: Also at St. Petersburg State Polytechnical University, St. Petersburg, Russia
41: Also at University of Florida, Gainesville, USA
42: Also at P.N. Lebedev Physical Institute, Moscow, Russia
43: Also at California Institute of Technology, Pasadena, USA
44: Also at Budker Institute of Nuclear Physics, Novosibirsk, Russia
45: Also at Faculty of Physics, University of Belgrade, Belgrade, Serbia
46: Also at University of Belgrade, Faculty of Physics and Vinca Institute of Nuclear Sciences, Belgrade, Serbia

47: Also at INFN Sezione di Pavia [a], Università di Pavia [b], Pavia, Italy
48: Also at National and Kapodistrian University of Athens, Athens, Greece
49: Also at Universität Zürich, Zurich, Switzerland
50: Also at Stefan Meyer Institute for Subatomic Physics (SMI), Vienna, Austria
51: Also at Adiyaman University, Adiyaman, Turkey
52: Also at Istanbul Aydin University, Istanbul, Turkey
53: Also at Mersin University, Mersin, Turkey
54: Also at Piri Reis University, Istanbul, Turkey
55: Also at Gaziosmanpasa University, Tokat, Turkey
56: Also at Ozyegin University, Istanbul, Turkey
57: Also at Izmir Institute of Technology, Izmir, Turkey
58: Also at Marmara University, Istanbul, Turkey
59: Also at Kafkas University, Kars, Turkey
60: Also at Istanbul University, Faculty of Science, Istanbul, Turkey
61: Also at Istanbul Bilgi University, Istanbul, Turkey
62: Also at Hacettepe University, Ankara, Turkey
63: Also at Rutherford Appleton Laboratory, Didcot, UK
64: Also at School of Physics and Astronomy, University of Southampton, Southampton, UK
65: Also at Monash University, Faculty of Science, Clayton, Australia
66: Also at Bethel University, St. Paul, USA
67: Also at Karamanoğlu Mehmetbey University, Karaman, Turkey
68: Also at Purdue University, West Lafayette, USA
69: Also at Beykent University, Istanbul, Turkey
70: Also at Bingol University, Bingol, Turkey
71: Also at Sinop University, Sinop, Turkey
72: Also at Mimar Sinan University, Istanbul, Istanbul, Turkey
73: Also at Texas A&M University at Qatar, Doha, Qatar
74: Also at Kyungpook National University, Daegu, Korea
75: Also at University of Hyderabad, Hyderabad, India